CYTOKINE CATCH-AND-RELEASE COMMUNICATION ENABLES LONG-TERM RESPONSE TO TRANSIENT INFLAMMATION

A Dissertation

Presented to the Faculty of the Weill Cornell Graduate School

of Medical Sciences

in Partial Fulfillment of the Requirements for the Degree of

Doctor of Philosophy

by

Jennifer Erin Oyler

August 2016

CYTOKINE CATCH-AND-RELEASE COMMUNICATION ENABLES LONG-TERM RESPONSE TO TRANSIENT INFLAMMATION

Jennifer Erin Oyler, Ph.D.

Cornell University 2016

In every biological system, individual cells must adapt to ever-changing environments in order to survive. To adapt, cells translate extra-cellular cues, into phenotypic changes. In the mammalian immune system, cells sample the environment for pathogens or tumors, and secrete cytokines to alert other cells of the threat. Genome-wide profiling techniques have been instrumental to determine the identity of genes that change in response to cytokines. Often these experiments profile mRNA before and after cytokine stimulation at a single time-point. While single time-point experiments are ideal for identifying which genes changed in response to a cytokine, studies of gene expression changes over time - dynamics - can reveal novel mechanisms of gene regulation. *In vivo*, cytokines are often secreted transiently (hours), yet the dynamics of an acute immune response occur over a week. These widely varied timescales pose a question: how do cells translate short-lived cytokine exposure into long-term gene expression changes that persist for the duration of an immune response? More fundamentally, what mechanisms exist to regulate the duration of a cells? response to a transient stimulus? We studied the transcriptional dynamics of cells exposed to a brief pulse of the cytokine Interferon γ and observed long-term up-regulation of genes in the antigen processing and presentation pathway. Transcription of these genes persisted over a timescale of 2 days, before slowly decaying after about one week. By combining mathematical modeling with a variety of experimental techniques, we learned that

IFNγ is captured by cell surface exposed phosphatidylserine on viable cells. The cytokine is then slowly released to drive persistent transcription of IFNγ-response genes in both an autocrine and paracrine manner. Ultimately, this enables a transiently produced cytokine to act over a timescale much longer than that of its secretion. This mechanism is a novel mode of cell-to-cell communication, which we coined catch-and-release communication. We observed that catch-and-release communication is a general phenomenon of cell-to-cell communication as it is applicable also to the cytokines Interleukin 12 and 23, and can be executed by diverse cell types from multiple different species. Functionally, catch-and-release signaling could enable cells separated by both space and time to communicate with one another.

BIOGRAPHICAL SKETCH

Jennifer graduated from Saint Joseph's University in 2009 with a Bachelors of Science, major in Biology and minor in Philosophy. She then spent several years as a research technician at the University of Pennsylvania Perelman School of Medicine under the supervision of Drs. Jeffrey Weiser and Michael Bachman. In 2011, Jennifer enrolled in the Immunology and Microbial Pathogenesis program at Weill Cornell Medical College, where she conducted doctoral work with Dr. Grégoire Altan-Bonnet.

ACKNOWLEDGEMENTS

I would first like to thank my thesis advisor, Grégoire Altan-Bonnet for his mentorship. Grégoire provided endless guidance and encouragement. In addition, Grégoire pushed me to step outside of my comfort zones and learn how to program, to write mathematical models, and to try new techniques.

I would also like to thank members of my thesis committee: Drs. Christina Leslie, João Xavier, and Jedd Wolchok. These individuals provided wonderful support and offered invaluable insights to our project during our many meetings over the past several years.

I would next like to thank members of the Altan-Bonnet lab, both past and present. First, thank you to Karen Tkach, Jesse Cotari, and Guillaume Voisinne for mentoring me during my early years in the lab. Karen especially taught me a range of experimental techniques and helped me navigate graduate school life. I would also like to thank Carly Ziegler, Amir Erez, Robert Vogel, and Ben Whitlock for the thoughtful insights and creative ideas they offered to me during the course of my project.

Additionally, I would like to thank Mojdeh Shakiba for her work on my project. Mojdeh's results were crucial for our understanding of the catch-and-release signaling mechanism. Thank you also to Nina Min for her work on my project. Nina contributed much of the data pertaining to IL12 and IL23 interactions with PS. Thanks to Carlos Carmona-Fontaine for help with microscopy and excellent barbecues. Also thanks to Nihal Altan-Bonnet, Oleg Krichevsky, and Taha Merghoub for their thoughtful insights into my project over the years and generous sharing of equipment and reagents.

I would also like to thank my first advisors in science - Dr. Eileen Grogan of Saint Joseph's University and Dr. Michael Bachman of the University of Michigan.

These two inspired my love of science and encouraged me to pursue graduate school.

I am endlessly grateful to my graduate school friends for providing new ideas, helping me troubleshoot experiments, and always being ready for a beer after lab: Clarissa Campbell-Menezes, Joris van der Veeken, Dane Samilo, Shashirekha Mundhra, Asaf Poran, Kerry Boyle, Carlos Carmona-Fontaine, Nicole Malandro, Ben Whitlock, and Mojdeh Shakiba.

Lastly, I would like to thank my family. First to my parents and my sister - Karen, Ralph, and Sarah Oyler - because they nurtured me in science from childhood and supported me through every challenge I have faced since. Finally, to Alon Oyler-Yaniv. Everything I learned and achieved in graduate school was due to his love, support, encouragement, and creativity. It is because of Alon that my project has developed into something I am so very proud of.

TABLE OF CONTENTS

LIST OF FIGURES

LIST OF TABLES

CHAPTER 1

INTRODUCTION

In every biological system, individual cells must adapt to ever-changing environments in order to survive. To adapt, cells respond to extra-cellular cues, which are translated into phenotypic changes. In the mammalian immune system, cells constantly sample the environment for potential pathogens or tumors, and then secrete small molecules called cytokines to alert surrounding cells of the threat. Many different cytokines exist which serve to communicate the particular immune context. For example, viral versus bacterial infections necessitate different cellular responses, thus different cytokines will be produced. Different cytokine cocktails elicit variable gene expression responses. Therefore diverse cell functions can be engineered based on the diversity of cytokines in the microenvironment. Indeed, a major focus of work has been deciphering which genes change in response to specific cytokines.

Genome-wide profiling techniques have been instrumental in determining the identity of genes that change in response to specific cytokines [14, 15]. Often these experiments profile mRNA derived from animal tissue or cultured cells before and after cytokine stimulation at a single timepoint. In addition, a great deal has been learned from experiments analyzing gene expression patterns in animals or humans that are deficient for components of cytokine signaling pathways [3, 18, 37, 65]. While these single, snapshot-type experiments are ideal for identifying which genes changed in response to a cytokine, studies of gene expression changes over time, dynamics, can reveal novel mechanisms of gene regulation [30, 31, 55, 68, 84].

Studying transcriptional dynamics has been a useful strategy to learn what general principles regulate gene expression. In a series of studies, cells were exposed

to a consistent source of the pro-inflammatory cytokine tumor necrosis factor α (TNFα), and RNA was harvested periodically and analyzed by either microarray or RT-qPCR [30, 31]. Examination of the gene expression kinetics revealed distinct waves of transcription with clusters of genes peaking in expression at early, intermediate, or late timepoints. The authors performed a series of experiments which proved that the basis for this clustering was largely inherent to the DNA and RNA code. Specifically, the time required for processing of pre-mRNA into mature mRNA (splicing rate) and the mature mRNA stability (biochemical degradation rate) were critical parameters controlling the transcriptional dynamics. The era of genome-wide studies and an appreciation for the importance of studying how systems change over time, have added complexity to datasets. This has necessitated the development of computational tools that make it easier (or even possible), to distill key features from large, multi-dimensional datasets.

In some cases, simple mathematical models can be useful tools that reveal insights that would otherwise be difficult or impossible to glean from complex datasets. For example, Rabani *et al.* implemented a mathematical model that did not assume that gene regulatory rates are constant with time [67, 68]. In other words, for a given gene, the rates of transcription, splicing, and mRNA degradation may change with time. A consequence of this is that a single transcriptional temporal pattern is achieved from many different regulatory strategies [68]. What is the purpose of using different strategies to achieve the same trajectory of gene expression? This question is ideally-suited for analysis with a mathematical model where testing of multiple hypotheses is quick, easy, and not subject to the constraints of what is experimentally possible. Simulations revealed that despite the ability of different regulatory strategies to achieve the same pattern of transcription, different strategies may have different functional roles. For instance, by increasing

all three rates (transcription, splicing, and degradation), a transcript achieves a similar temporal profile as a simple increase in transcription rate, yet in the former case, the level of gene expression is more robust to a noisy input signal compared to the latter.

Up-stream of gene expression, extracellular cues are encoded by signaling molecules and transcription factors. These molecules initiate intracellular signaling relays, ultimately resulting in changes in cell phenotype. The strategy of combining mathematical modeling with time-course experiments has proven especially fruitful for dissecting gene regulatory mechanisms from the kinetics of transcription factor activation. For example, signaling molecules can exhibit diverse dynamical patterns that drive variable kinetics of gene expression [10, 33, 46, 58, 59, 62, 66, 82, 85].

To take a classic example, Cai *et al.* studied the nuclear localization dynamics of the yeast transcription factor Crz1 in response to different doses of extracellular calcium [10]. The frequency of Crz1 nuclear localization was directly proportional to the calcium concentration. This was a novel way for cells to intracellularly encode the concentration of an extracellular stimulus. Traditionally, cells were thought to primarily encode the stimulus dose by tuning the amplitude of response or concentration of active transcription factor. To explore the functional significance of this, the authors used a mathematical model that compared expression of different genes given either amplitude or frequency modulation as a regulatory strategy. The model predicted that frequency modulation would enable cells to coordinate expression of different signal-response genes across variable stimulus doses. The authors tested this prediction experimentally and found that, indeed, frequency modulation of Crz1 localization enabled genes to be expressed proportionally across variable calcium doses, despite different promoter architecture.

These conclusions would have been impossible but for an experiment that tracked signaling dynamics and implementation of a model that generated a testable prediction. Understanding the myriad ways that healthy cells translate extracellular cues into phenotypic changes allows us to more clearly identify dysfunctional signaling in diseases like cancer [29]. In addition studying dynamics can have immediate practical implications.

In a recent example, tracking the signaling dynamics of the tumor suppressor p53 enabled identification of the optimal timing for administration of DNA damage to maximize tumor cell death [12]. The obvious goal of chemotherapy is to maximize killing of tumor cells, while sparing healthy cells. However, one major challenge of this goal is that upon administration of the drug, there are often subsets of cancer cells which survive. The authors hypothesized that by first sensitizing the tumor cells with a drug, they may be able to increase the tumors' susceptibility to subsequent administration of another drug. They discovered that following inhibition of the p53 suppressor MDMX, cells undergo an initial burst of p53 nuclear localization, followed by several periods of p53 nuclear-cytoplasmic oscillation. If a DNA damaging drug was applied during the early p53 burst, nearly all of the tumor cells died. In stark contrast, if the drug was applied during the oscillatory phase, nearly all of the tumor cells survived. The authors attributed this to different gene expression profiles during the p53 burst and oscillatory states. This observation argues that the timing of drug administration is a critical parameter that ought to be included when clinicians decide upon drug dosage and potential combination therapies.

In similar example, Lee *et al.* investigated the effectiveness of treating triple negative breast cancer cell lines with sequential application of first an epidermal

growth factor receptor inhibitor (erlotinib), followed by a DNA damaging drug [45]. Erlotinib alone was only modestly effective in killing the cells, and adding the DNA damaging agent 30 minutes after erlotinib did not enhance cytotoxicity. However, when cells were sensitized for a day with erlotinib, then subjected to DNA damage, cytotoxicity increased dramatically. The authors examined the changes in the signaling and gene expression network over time after erlotinib administration and noticed that the tumor cells slowly adopted a more "normal" phenotype and lost canonical oncogenic signatures. To parse the high-dimensional dataset they generated, the authors used linear models such as principle component analysis and partial least squares regression. Their models pointed to the importance of the pro-apoptotic gene caspase-8 in mediating cell death after erlotinib treatment. Indeed, when they knocked down caspase-8 prior to EGFR inhibition, DNA damage was less effective in killing the cells. Again, the authors would have not identified this drug synergy had they not investigated dynamics. In addition, the mechanism of caspase-8 activation would have been difficult to pinpoint without a model to reduce the complexity of their high-dimensional dataset.

DNA damaging agents such as chemotherapeutic drugs and/or radiation for cancer treatment have been joined recently by small molecule inhibitors designed to target specific pathways that are dysregulated in tumors. More recently, the immune system has been recognized as holding tremendous potential in the fight against cancer if it can be "unleashed" upon the tumor. Indeed, immunotherapeutics have been demonstrated to cause dramatic and durable remission in certain cancer subsets [27, 43, 64, 81]. Given that the timing and order of chemotherapeutic and small molecule inhibitor administration can be optimized [12, 45], we speculated that there is also an optimal timing for immunotherapeutic intervention after tumor exposure to pro-inflammatory cytokines.

The pro-inflammatory cytokine Interferonγ (IFNγ) is produced by activated immune cells, such as T cells and Natural Killer cells [73]. T cells scan host cells via T cell receptor (TCR) binding to peptides presented by either major histocompatibility complex class I or II (MHC-I or -II) on host cells. T cells are tolerized to self-peptides, but can become activated if their TCR binds to mutated or over-expressed self peptides (in the case of cancer), or pathogen-derived peptides. When a TCR binds strongly to peptide-MHC, it physically arrests, initiates a signaling cascade that results in gene expression changes, and secretes cytokines including IFNγ [34]. T cells and peptide-presenting host cells remain in physical contact for several hours while T cells secrete cytokines. After several hours, T cells up-regulate inhibitory molecules, causing them to dissociate from the host cells and cease cytokine production. Another group has more rigorously quantified the timescale of cytokine production [32]. In a population of T cells, the IFNγ production period follows a log normal distribution where cells secrete cytokine for 5.9 ± 3.6 hours after activation. It is worth noting that these several hours of cytokine secretion represent only a minuscule window of an overall acute immune response, which occurs over the timescale of approximately a week.

Mice and humans deficient for IFNγ signaling exhibit profound susceptibility to viruses, parasites, and bacteria. In addition, IFNγ prevents primary tumor development and improves rejection of established tumors [16, 78]. Across diverse human cancers, the presence of an IFNγ gene signature is a positive prognostic marker [49]. Importantly, after exposure to IFNγ, cells are better able to be recognized and killed by T cells, indicating that the cytokine "primes" cells for subsequent T cell encounter.

The timescale over which cells maintain a phenotypic change after exposure to

a transient signal can span several orders of magnitude (Figure 1.1).

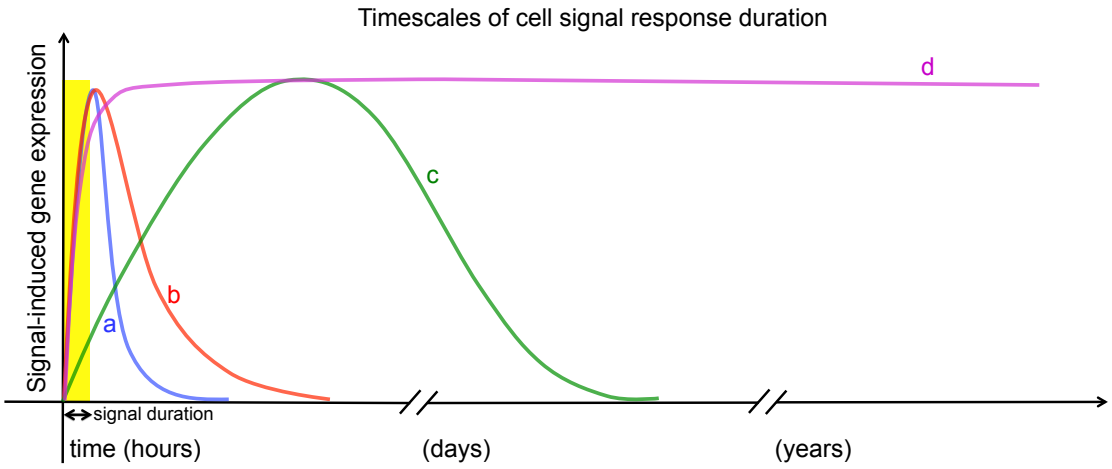

Figure 1.1: **Timescales of phenotypic change after exposure to transient stimulus.** In the simplest model of signal-induced gene up-regulation (a, blue), the timescale of gene up-regulation essentially tracks the presence of the external signal. Stabilization of mRNA would modestly lengthen the time required for gene expression to return to background levels, but would not change the peak time (b, red) [20]. Gene expression can change indefinitely in response to a transient signal resulting in cell differentiation (d, purple). This can be caused by an epigenetic change that chemically or structurally modifies the chromatin leading to sustained gene expression in the absence of the original signal [2]. Alternatively, positive feedback can trigger a switch that irreversibly alters the cell phenotype [39]. Mechanisms promoting an intermediate phenotype, where cells can amplify their timing of signal response past the timescale of the signal, but still return to their original cell state are understudied (c, green).

Given the most basic model of gene regulation (a, blue), the cells' response would essentially track the external stimulus. Once the signal is abrogated, the cell would rapidly return to its original phenotypic state. A mechanism that slows mRNA decay would modestly extend the time before a cell reached its original state, but ultimately the timescale of gene expression would coincide with the timescale of the signal (b, red) [20]. At the other end of the spectrum, chromatin modifications can stabilize gene expression in response to a signal such that the phenotypic change persists indefinitely (d, purple) [2]. Alternatively, phenotypic changes can

be maintained by biochemical switches caused by positive feedback [39]. How though, can cells achieve an intermediate response (c, green)? In this scheme, cells can extend their period of gene expression past the timescale of signal exposure, but retain the ability to return to return to their original phenotypic state. Examples of intermediate timescales of signal response are rare in the literature.

CHAPTER 2

IN THIS DISSERTATION

Given that IFNγ is secreted transiently (hours), yet is crucial for host-pathogen or host-tumor defense over long timescales (days/weeks), we sought to determine the temporal duration of a cells response to brief IFNγ exposure. Furthermore, we asked what regulatory strategies control how long a cell responds to IFNγ. The aims generated by these two over-arching questions will be outlined in the next section.

2.1 Aims

1. Determine the timing after IFNγ exposure when melanoma cells best activate T cells.
2. Quantify the temporal duration of the cell gene expression response to transient IFNγ.
3. Characterize the gene expression signature of melanoma cells following transient exposure to IFNγ.
4. Identify the molecular mechanism(s) that regulate the temporal duration of the melanoma response to transient IFNγ.

CHAPTER 3

A MINIMAL MODEL OF GENE EXPRESSION BASED ON THE CENTRAL DOGMA OF BIOLOGY.

We introduce a minimal model for the cell response to an external stimulus. The kinetics of the reaction can be summarized as:

$$\frac{dX}{dt} = k(t) - \beta \cdot X, \tag{3.1}$$

where $X(t)$ is a cell response (i.e. mRNA level) as a function of time, $k(t)$ is the response rate (transcription rate), and β is the constant molecular decay rate for the response.

We introduce a binary signal at time $t = 0$ and remove it at time $t = t_0$. Under the simplest assumptions, the transcription rate changes with the introduction of the signal, and returns to its original baseline value once the signal is removed (Figure 3.1):

$$k(t) = \begin{cases} k_0 & \text{if } 0 < t \\ k_1 & \text{if } 0 < t < t_0 \\ k_0 & \text{if } t_0 < t \end{cases}. \tag{3.2}$$

The resulting dynamics of X is an exponential approach while the signal is supplied, followed by an exponential decay back to its baseline (Figure 3.1):

$$X(t) = \begin{cases} \frac{k_0}{\beta} \quad \text{(baseline value)} & \text{if } t < 0 \\ \frac{k_0}{\beta} + \frac{k_1 - k_0}{\beta}\left(1 - e^{-\beta t}\right) & \text{if } 0 < t < t_0 \\ \frac{k_0}{\beta} + \frac{k_1 - k_0}{\beta}\left(1 - e^{-\beta t_0}\right) e^{-\beta(t - t_0)} & \text{for } t_0 < t \end{cases} \tag{3.3}$$

Notice that while a decrease in the molecular decay rate β might prolong the signal, the functional form of transcriptional dynamics remains unchanged. Response increases while the signal is supplied, peaks when the signal is removed, and decays back to the baseline after. In this system, there is only a single timescale which is set by the molecular decay rate, β.

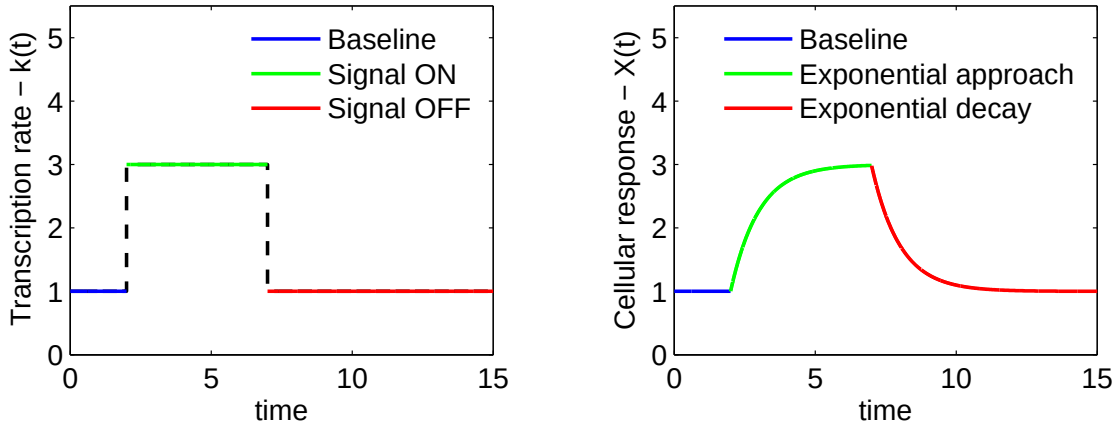

Figure 3.1: **Exposure to a transient signal given the simplest model of gene expression.** The transcription factor is expected to change instantaneously in response to the signal. The transcriptional response is expected to follow an exponential approach following application of signal, and to degrade exponentially back to the steady state level after removal of the signal.

3.1 Specifying the model for the IFNγ response.

We begin our model of transcription with the central dogma of molecular biology: DNA is transcribed into mRNA at a rate $k_{\text{transcription}}$, and mRNA chemically degrades over time. This is summarized in the equation:

$$\frac{d[\text{mRNA}]}{dt} = k^{\text{basal}}_{\text{transcription}} - [\text{mRNA}] \cdot k_{\text{decay}}, \tag{3.4}$$

The steady state $\left(\frac{d[\text{mRNA}]}{dt} = 0\right)$ concentration of mRNA in the system is $[\text{mRNA}]_{\text{ss}} = \frac{k^{\text{basal}}_{\text{transcription}}}{k_{\text{decay}}}$.

The effect of IFNγ on transcription is introduced by the transcription factor STAT1. When IFNγ binds to its receptor, STAT1 is phosphorylated by Janus Kinase (JAK), dimerizes, and translocates to the nucleus. These processes are summarized by the following set of equations,

$$\begin{cases} \frac{d[\text{IFN}\gamma R_c]}{dt} = k_{\text{on}} \cdot [\text{IFN}\gamma R] \cdot [\text{IFN}\gamma] - k_{\text{off}} \cdot [\text{IFN}\gamma R_c], \\ \frac{d[\text{IFN}\gamma R]}{dt} = -\frac{d[\text{IFN}\gamma R_c]}{dt}, \\ \frac{d[\text{pSTAT1}]}{dt} = k_{\text{phos}} \cdot [\text{STAT1}] \cdot [\text{IFN}\gamma R_c] - k_{\text{deg}} \cdot [\text{pSTAT1}], \\ \frac{d[\text{STAT1}]}{dt} = -\frac{d[\text{pSTAT1}]}{dt}, \end{cases} \tag{3.5}$$

where IFNγR is the IFNγ receptor, IFNγR_c is the complex of IFNγ and its receptor, k_{on} and k_{off} are the kinetic on- and off- rates of the IFNγR_c complex formation, and k_{phos} and k_{deg} are the STAT1 phosphorylation and degradation rates.

Experimentally, we checked that STAT1 phosphorylation occurs rapidly upon exposure of the cells to IFNγ (Figure 3.2a), reaching a steady state within minutes. Following treatment with a JAK inhibitor, pSTAT1 levels in the system rapidly return to baseline levels (Figure 3.2b).

Given that the timescale of transcription is on the order of hours-days compared to the timescale of signaling (seconds-minutes), for simplicity, the dynamics of STAT1 phosphorylation and dephosphorylation are assumed to reach steady state instantaneously.

Using conservation:

$$\begin{aligned} \text{IFN}\gamma R_{\text{total}} &= \text{IFN}\gamma R + \text{IFN}\gamma R_c, \\ \text{STAT1}_{\text{total}} &= \text{STAT1} + \text{pSTAT1}, \end{aligned} \tag{3.6}$$

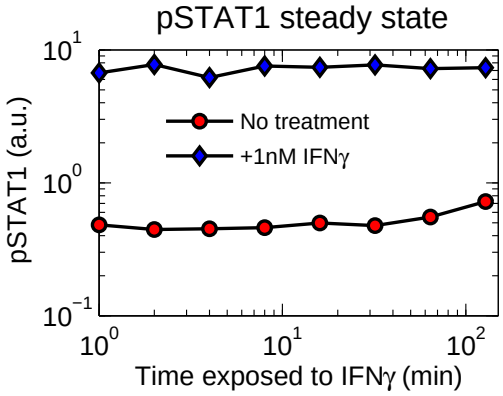

(a) **pSTAT1 signaling rapidly reaches steady-state after cell exposure to IFNγ.** B16 cells were exposed to either media alone, or 1nM IFNγ. Cells were harvested at indicated timepoints, fixed and permeabilized, and stained for phosphorylated STAT1 protein. Fluorescence was quantified by flow cytometry.

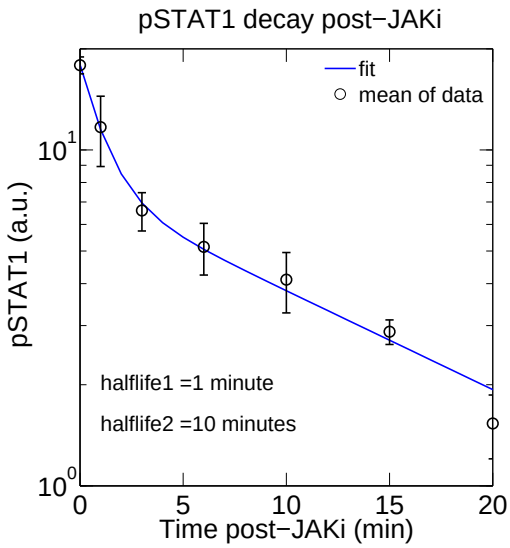

(b) **pSTAT1 signaling rapidly returns to baseline upon administration of a JAK inhibitor.** Cells were stimulated with 10nM IFNγ, then 10μM of the JAK1/2 inhibitor AZD1480 was added. Cells were harvested at indicated timepoints, fixed and permeabilized, and stained for pSTAT1. The data were fit with a double exponential decay function with the decay rates for each exponent as fitting parameters. Data plotted is the mean and s.e.m. (errorbars) and representative of 3 independent experiments.

Figure 3.2: Timescales of the pSTAT1 response to signals.

where IFNγR_{total}, and $\text{STAT1}_{\text{total}}$ are the total levels of IFNγ receptor and STAT1, respectively.

From these equations, we calculate the steady-state of IFNγR_c and pSTAT1 for a given dose of IFNγ:

$$
\begin{aligned}
\mathrm{IFN}\gamma R_c &= \mathrm{IFN}\gamma R_{\mathrm{total}} \frac{k_{\mathrm{on}} \cdot [\mathrm{IFN}\gamma]}{(k_{\mathrm{on}} \cdot [\mathrm{IFN}\gamma]) + k_{\mathrm{off}}} \propto \frac{1}{1 + \frac{K_D}{[\mathrm{IFN}\gamma]}} \\
\mathrm{pSTAT1} &= \frac{[\mathrm{IFN}\gamma R_{\mathrm{total}}][\mathrm{STAT1}_{\mathrm{total}}] k_{\mathrm{phos}} k_{\mathrm{on}}}{[\mathrm{IFN}\gamma R_{\mathrm{total}}] k_{\mathrm{on}} k_{\mathrm{phos}} + k_{\mathrm{deg}} k_{\mathrm{on}}} \left(\frac{[\mathrm{IFN}\gamma]}{[\mathrm{IFN}\gamma] + \frac{k_{\mathrm{deg}} k_{\mathrm{off}}}{[\mathrm{IFN}\gamma R_{\mathrm{total}}] k_{\mathrm{on}} k_{\mathrm{phos}} + k_{\mathrm{deg}} k_{\mathrm{on}}}} \right) \\
&\propto \frac{1}{1 + \frac{\mathrm{EC}_{50}}{[\mathrm{IFN}\gamma]}},
\end{aligned}
\tag{3.7}
$$

where $K_d = \frac{k_{\mathrm{off}}}{k_{\mathrm{on}}}$. The dose dependance of pSTAT1 on IFNγ concentrations is expected to follow a Hill function with coefficient 1. (Figure 7.25a) shows that cells indeed follow such a dose response curve with $\mathrm{EC}_{50} \approx 3\mathrm{pM}$:

$$
\mathrm{pSTAT1}([\mathrm{IFN}\gamma]) \propto \frac{1}{1 + \frac{\mathrm{EC}_{50}}{[\mathrm{IFN}\gamma]}}. \tag{3.8}
$$

3.2 Linking transcription factor activation with transcription.

Next, we will explore how exposure to IFNγ would affect transcription. By exposing cells to a constant, saturating concentration of IFNγ, we can assess how the rate of transcription changes with time.

$$
k_{\mathrm{transcription}}(t) = \frac{d[\mathrm{mRNA}]}{dt} + [\mathrm{mRNA}] \cdot k_{\mathrm{decay}}. \tag{3.9}
$$

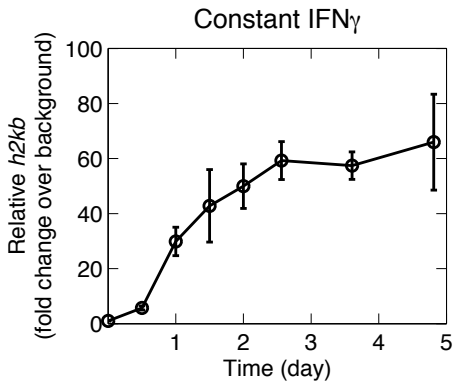

(a) **The transcriptional response to constant, saturating IFNγ.** B16 cells were exposed to a constant concentration of 10nM IFNγ. RNA was harvested periodically and the kinetics of *h2kb* transcript accumulation were quantified by RT-qPCR. The data plotted is the mean and s.e.m (errorbars) and representative of at least 3 independent experiments.

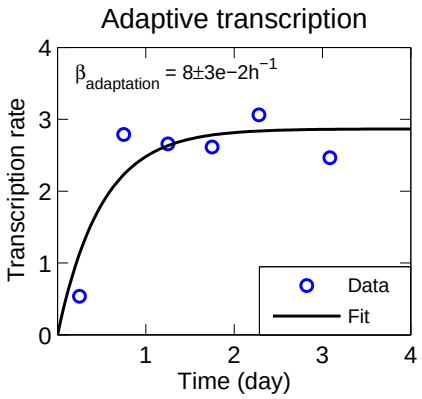

(b) **The transcription rate yields the adaptation timescale.** The transcription kinetics were converted into the transcription rate using Equation 3.9. This curve was fit with an exponential approach and the adaptation timescale was computed from the fit.

Figure 3.3: Accounting for a transcriptional lag (adaptation time) after initiation of the signaling response.

(Figure 3.3a) shows how the rate of transcription changes following IFNγ exposure. We observed an adaptation period where transcription increases before reaching a new elevated constant rate (Figure 3.3b). These dynamics can be approximated by an exponential approach with timescale $\tau_{\text{adaptation}} = \frac{1}{\beta_{\text{adaptation}}} \approx 12h$. Moreover, the new, elevated, steady state is pSTAT1 dependent, with higher levels of pSTAT1 translating to an increased transcription rate. In our model, we assume pSTAT1 linearly increases the maximal transcription rate:

$$k_{\text{transcription}} \rightarrow \; k^{\text{basal}}_{\text{transcription}} + \; \alpha_p \left(1 - \exp\left(-\beta_{\text{adaptation}} t\right)\right) \text{pSTAT1},$$

where the constant α_p represents the proportionality between increase in transcription and pSTAT1. The updated transcription equation (3.4) is now:

$$\frac{d[\text{mRNA}]}{dt} = k^{\text{basal}}_{\text{transcription}} + \alpha_p \left(1 - \exp\left(-\beta_{\text{adaptation}} \cdot t\right)\right) \text{pSTAT1} - [\text{mRNA}] \cdot k_{\text{decay}}. \tag{3.10}$$

We will next present solutions for this equation under different conditions.

3.3 Exposure to constant IFNγ.

When cells are exposed to a constant concentration of IFNγ, the solution to equation 3.10 is approximately a bounded exponential growth with an asymptote at $[\text{mRNA}]([\text{IFN}\gamma])_{\text{asympt}} = \frac{k_{\text{transcription}} + \alpha_p \cdot \text{pSTAT1}([\text{IFN}\gamma])}{k_{\text{decay}}}$.

$$\begin{aligned}[\text{mRNA}](t, [\text{IFN}\gamma]) =& \frac{k^{\text{basal}}_{\text{transcription}} + \alpha_p \cdot \text{pSTAT1}([\text{IFN}\gamma])}{k_{\text{decay}}} \\ &- \frac{\alpha_p \cdot \text{pSTAT1}([\text{IFN}\gamma])}{k_{\text{decay}} - \beta_{\text{adaptation}}} \exp\left(-\beta_{\text{adaptation}} t\right) \\ &+ \frac{\alpha_p \cdot \text{pSTAT1}([\text{IFN}\gamma]) \beta_{\text{adaptation}}}{k_{\text{decay}}\left(k_{\text{decay}} - \beta_{\text{adaptation}}\right)} \exp\left(-k_{\text{decay}} t\right)\end{aligned} \tag{3.11}$$

3.4 Exposure to transient IFNγ.

Next, we solve the equation assuming transient exposure to IFNγ ($0 < t < t_0$). Initially, as for the constant case, there is an exponential approach to an elevated state. Once IFNγ is removed, mRNA levels exponentially decrease back to their original level of $\frac{k^{\text{basal}}_{\text{transcription}}}{k_{\text{decay}}}$ (Figure 3.4).

$$[\text{mRNA}](t, t_0, [\text{IFN}\gamma]) = \begin{cases} \frac{k^{\text{basal}}_{\text{transcription}} + \alpha_p \cdot \text{pSTAT1}([\text{IFN}\gamma])}{k_{\text{decay}}} - \frac{\alpha_p \cdot \text{pSTAT1}([\text{IFN}\gamma])}{k_{\text{decay}} - \beta_{\text{adaptation}}} e^{-\beta_{\text{adaptation}} t} \ldots \\ + \frac{\alpha_p \cdot \text{pSTAT1}([\text{IFN}\gamma]) \beta_{\text{adaptation}}}{k_{\text{decay}} \left(k_{\text{decay}} - \beta_{\text{adaptation}}\right)} e^{-k_{\text{decay}} t} & \text{for } 0 < t < t_0 \\ \frac{k^{\text{basal}}_{\text{transcription}}}{k_{\text{decay}}} + \left(\frac{\alpha_p \cdot \text{pSTAT1}([\text{IFN}\gamma])}{k_{\text{decay}}} - \frac{\alpha_p \cdot \text{pSTAT1}([\text{IFN}\gamma])}{k_{\text{decay}} - \beta_{\text{adaptation}}} e^{-\beta_{\text{adaptation}} t_0} \ldots \right. \\ \left. + \frac{\alpha_p \cdot \text{pSTAT1}([\text{IFN}\gamma]) \beta_{\text{adaptation}}}{k_{\text{decay}} \left(k_{\text{decay}} - \beta_{\text{adaptation}}\right)} e^{-k_{\text{decay}} t_0} \right) e^{-k_{\text{decay}} (t - t_0)} & \text{for } t_0 < t \end{cases} \tag{3.12}$$

A key feature of these dynamics is that under these considerations the time of maximal mRNA level, t_{max}, is equal to the time of signal termination ($t_{\text{max}} = t_0$), regardless of any parameter choice.

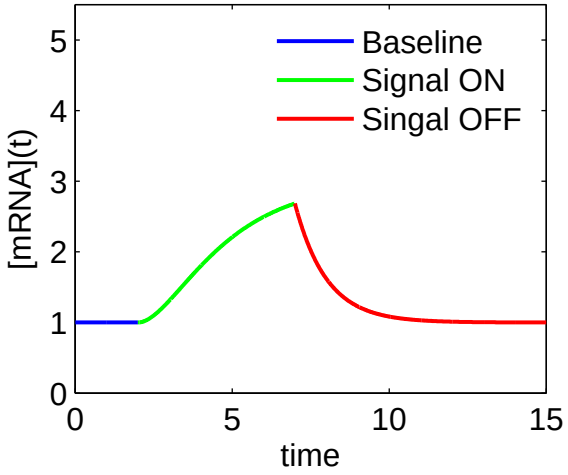

Figure 3.4: **Exposure to transient IFNγ given the simplest model of gene expression.** pSTAT1 is expected to change instantaneously in response to IFNγ. The transcriptional response is expected to follow an exponential approach with a transcriptional adaptation time following application of IFNγ, and to degrade exponentially back to the steady state level after removal of the cytokine.

3.5 Model parameters

Our mathematical modeling relies on rigorous parameterization. All of the parameters in our model are either published, or have been experimentally checked by us. Some of the parameters below are used exclusively for the updated version of the mathematical model introduced later in the dissertation.

Table 3.1: Parameters used to model the dynamics of our system.

Parameter	Value	Unit	Source
EC_{50}	2.7±1	pM	Figure 7.25a
k^X_{catch}	$1.2 \pm 0.1 \cdot 10^5$	$M^{-1}s^{-1}$	Inferred from Figure 7.24 and 7.27
k^X_{release}	$3.7 \pm 0.4 \cdot 10^{-5}$	s^{-1}	Figure 7.27
k_{removal}	24	h^{-1}	Our experiments (data not shown)
$k^{\text{mRNA}}_{\text{decay}}$	$2.9 \cdot 10^{-2}$	h^{-1}	[75]
$k^{\text{protein}}_{\text{decay}}$	$2.3 \cdot 10^{-1}$	h^{-1}	[75]
$k_{\text{translation}}$	0.1	$mRNA^{-1}{\cdot}s^{-1}$	[75]
$\beta_{\text{adaptation}}$	$8 \pm 3 \cdot 10^{-2}$	h^{-1}	Figure 3.3a Figure 3.3b
k^R_{on}	$7.3 \cdot 10^6$	$M^{-1}s^{-1}$	[71]
k^R_{off}	$5 \cdot 10^{-3}$	s^{-1}	[71]
IFNγR	$2 \cdot 10^3$	molecules·$cell^{-1}$	[13]
X	4700 ± 800	molecules·$cell^{-1}$	Fit in this study

CHAPTER 4

DETERMINING THE TIMING AFTER IFNγ EXPOSURE WHEN MELANOMA CELLS BEST ACTIVATE T CELLS.

We sought to quantify the timescale of a cells response to transient IFNγ. Exposure of cells to IFNγ is known to increase their recognition and killing by T cells [73]. We quantitatively tested this observation by creating an assay that functionally reports when IFNγ-pulsed cells are most sensitive to T cell recognition. B16 mouse melanoma cells were pulsed briefly (5h) with IFNγ, then washed and cultured in cytokine-free conditions (Figure 4.1a). Subsequent to IFNγ exposure, pmel T cells were added to the culture and their activation was quantified by measuring cytokine secretion. Pmel CD8+ T cells specifically recognize the endogenously-expressed gp100 peptide antigen presented by MHC-I on melanoma cells (Figure 4.1b) [60].

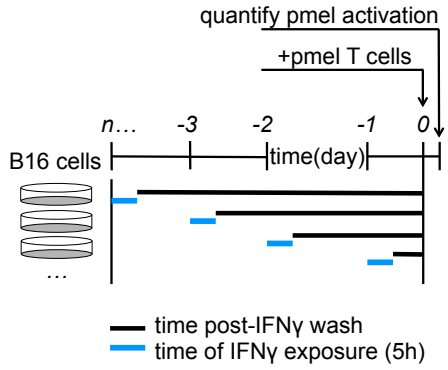

(a) **Diagram of experimental setup.** Different flasks of B16 cells were pulsed daily for 5h with 10nM IFNγ, then washed thoroughly. After 7 days, day 5 pmel blasts were co-cultured with an equal number of B16 cells for 7 hours, and pmel activation was quantified by Miltenyi IFNγ cytokine secretion assays.

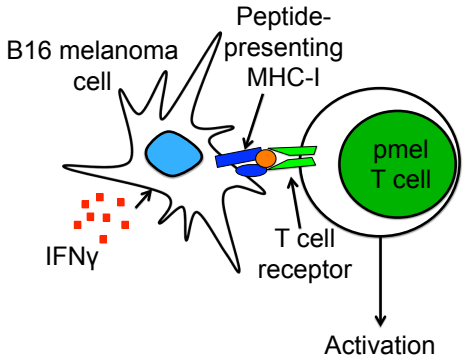

(b) **Cartoon of the experimental system.** B16 mouse melanoma cells present the endogenous melanoma differentiation antigen gp100 by MHC-I (H2-D^b). Pmel CD8+ T cells have a transgenic TCR specific for gp100 presented in the context of MHC-I.

Figure 4.1: Diagrams outlining the B16 mouse melanoma-Pmel system and experimental setup

IFNγ-pulsed melanoma cells increased over time in their capacity to activate T cells, peaking around two days post-exposure (Figure 4.2). By 5-7 days the capacity of B16 cells to activate T cells returned to pre-treatment levels. The observation that T cell activation peaked at two days implied that B16 cells persistently up-regulated cytokine-response genes for days after removal of the original signal.

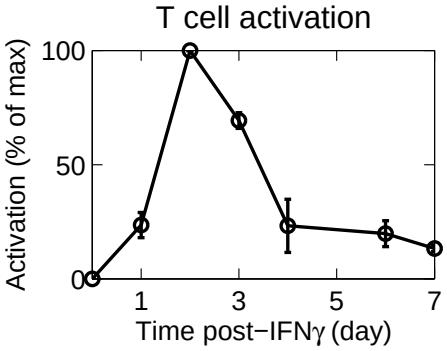

Figure 4.2: **B16 cells best activate T cells 2 days after their initial exposure to IFNγ** Pmel production of IFNγ was used as a readout of activation and quantified by flow cytometry. Data plotted is the mean and s.e.m. (errorbars) and representative of 3 independent experiments.

It is worth noting that the actual magnitude of T cell activation in these experiments is small. After seven hours of co-culture, only about $3-5\%$ of the total T cells in the culture become activated (IFNγ+). If the T cells are naive at the time of co-culture, activation does not occur for any cells over the 7 hour period for any marker of activation, including Interleukin 2 receptorα up-regulation, CD69 up-regulation, or phosphorylation of Erk protein (data not shown). Why is the activation in our system so weak? Many immunological assays make use of transgenic T cell receptors and engineered antigens. An example of one such system is the OT-1 - ovalbumin (OVA) system where the T cell receptor specifically recognizes an OVA-derived peptide when presented in the context of MHC-I. OVA is a non-self derived peptide and is therefore often introduced into antigen presenting cells by exposing the cells to a large dose of exogenous OVA. In these experiments

it is not unusual to observe a large fraction of activated T cells in the cultures due to both the strength of the T cell receptor - peptide MHC interaction, and also to the abundance of OVA after antigen presenting cells are pulsed with it. Gp100 is a natural, endogenous peptide and is therefore presented at much lower frequency than if cells were pulsed with a high concentration of free peptide. In addition, gp100 is a self-derived peptide - a melanocyte differentiation antigen, thus the strength of T cell receptor interaction is much weaker. Taken together, we actually view the weak activation observed in our assays as a strength of our system, because it more faithfully recapitulates what is likely to occur *in vivo* during an actual T cell response to melanoma.

We hypothesized that genes in the antigen presentation cluster caused the pattern of T cell activation that we observed. To test this, we repeated our T cell activation assay with several additional conditions (Figure 4.3a). To a second group of melanoma cells, we blocked MHC-I-T cell receptor interaction with a neutralizing antibody. Additionally, EL4 mouse thymoma cells, which possess the appropriate MHC-I haplotype but lack the specific peptide antigen were pulsed with IFNγ and cultured with T cells. After exposure to IFNγ, EL4 cells up-regulated MHC-I approximately 3-fold, indicating that they do respond to the cytokine (not shown). T cell activation was completely abrogated when MHC-I was blocked, or in the absence of peptide antigen in the case of EL4 cells (Figure 4.3b). Together, these data show that the long-term pattern of T cell activation after brief exposure to IFNγ is peptide-specific, and dependent on the MHC class I antigen presentation pathway.

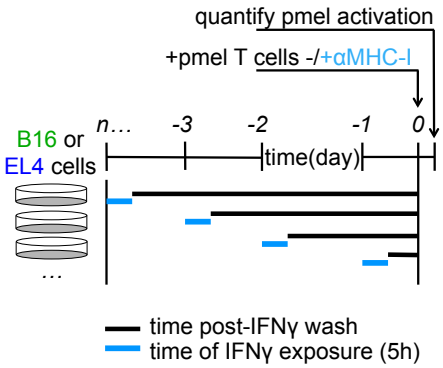

(a) **Diagram of experimental setup.** Different flasks of B16 or EL4 cells were pulsed daily for 5h with 10nM IFNγ, then washed thoroughly. After 7 days, day 5 pmel blasts were co-cultured with an equal number of B16 or EL4 cells, and pmel activation was quantified by cytokine secretion assays. An additional cohort of B16-pmel co-cultures received neutralizing antibodies directed against MHC-I, disrupting TCR-MHC-I interactions.

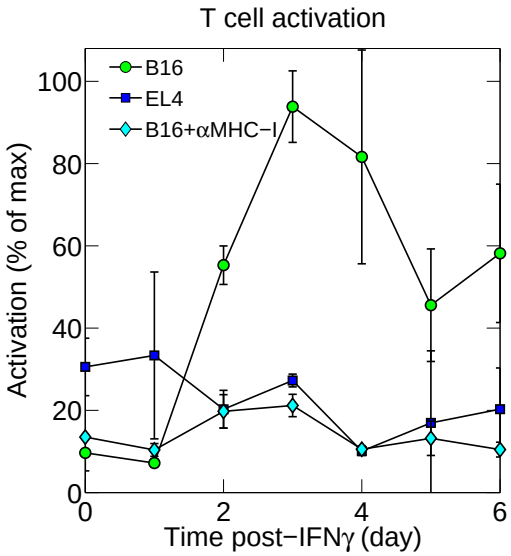

(b) **The pattern of T cell activation is MHC-I and peptide-dependent** Pmel production of IFNγ was used as a readout of activation and quantified by flow cytometry. Data plotted is the mean and s.e.m. (errorbars) and representative of 2 independent experiments.

Figure 4.3: The delayed pattern of T cell activation is MHC-I and peptide-dependent

CHAPTER 5

QUANTIFYING THE TEMPORAL DURATION OF THE CELL GENE EXPRESSION RESPONSE TO TRANSIENT IFNγ.

We reasoned that the time points when melanoma cells best-activated T cells would coincide with their peak expression of IFNγ-response genes. To check whether the dynamics of IFNγ-response genes matched those of T cell activation, we quantified mRNA from melanoma cells using RNA-sequencing for several days after IFNγ exposure. We used RNA-seq to gain a genome-wide view of the melanoma response to transient IFNγ.

To perform this experiment, B16 melanoma cells were either mock-treated or pulsed with 10nM IFNγ for 5h, then thoroughly washed. RNA was then harvested and purified at the indicated timepoints. The Integrated Genomics Organization at Memorial Sloan Kettering Cancer Center (MSKCC) performed quality checks on our purified RNA to ensure that it was of sufficient quality to proceed, then prepared a library of complementary DNA (cDNA), and performed sequencing. The resulting reads were aligned by the Bioinformatics core facility at MSKCC. We carried out the remaining bioinformatics analysis using MATLAB software. Figure 5.1 details the process of filtering genes. In addition, filtering is explained in further detail in the following paragraph.

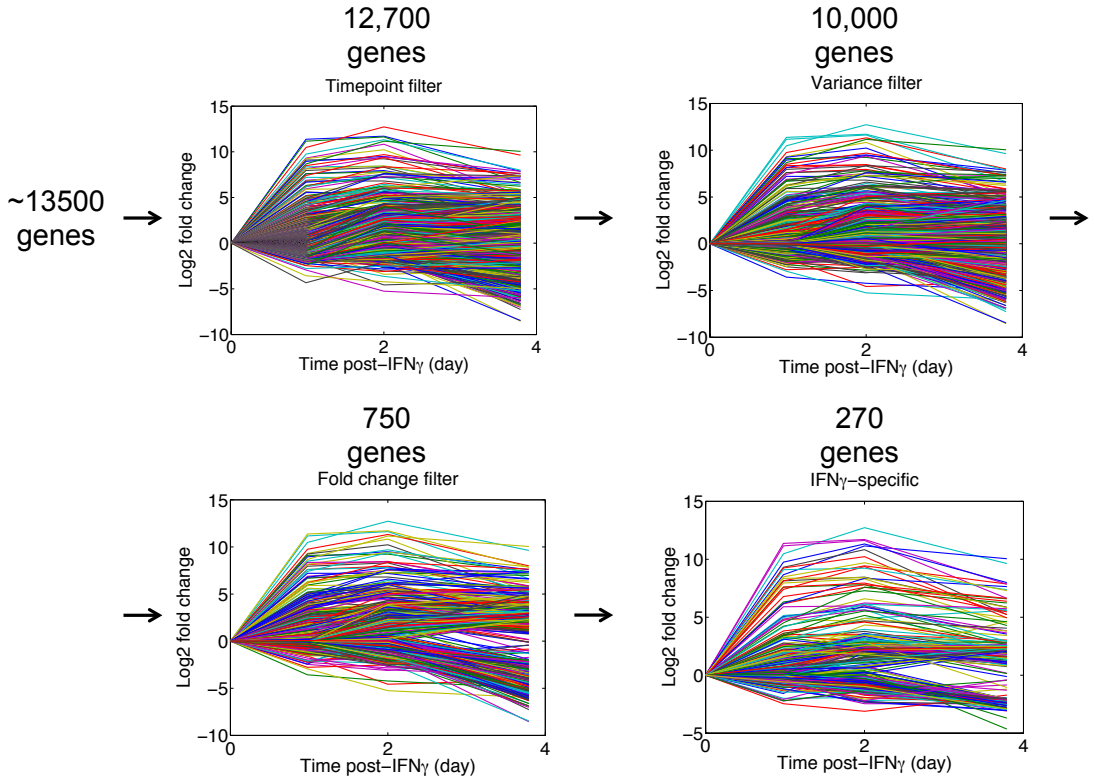

Figure 5.1: **Bioinformatic pipeline** Each line shows the mean of duplicate RNA samples and the dataset shown represents the IFNγ dataset as an example. For each dataset (IFNγ-pulsed and mock-pulsed), genes were first filtered based on their inclusion in all timepoints. Next, genes were filtered based on variance and then based on fold change. Finally, all genes which remained in the mock-treated condition and also in the IFNγ condition were removed from the IFNγ dataset.

At first, each dataset (mock-treated or IFNγ-pulsed) contained about 13,500 genes. For both datasets, we removed genes which did not have all timepoints. This eliminated about 5% of the total genes. Genes were then masked based on variance using the MATLAB function genevarfilter. This function ranks the variance between transcript expression at each timepoint and eliminates genes which fall into the bottom 20%, essentially removing all genes which stay relatively static over time. Next, the remaining genes were filtered based on their degree of up- or down-regulation. Any genes which were not up- or down-regulated by at least 4 fold were removed, leaving us with about 7% of the remaining genes.

Finally, all genes which remained in the IFNγ-pulsed dataset that were also present in the mock-treated control group were eliminated. This analysis left us with 271 genes which changed specifically, and significantly in response to transient IFNγ treatment.

Our next goal was to identify the major classes of transcriptional dynamics in response to IFNγ. Our assumption was that the unifying feature of each transcriptional class would be the mode of gene regulation. In other words, we predicted that genes that clustered together would be regulated similarly. Tavazoie *et al.* used the k-means algorithm to cluster sequencing data obtained from synchronized yeast cultures to identify classes of transcriptional dynamics [84]. They predicted that each class would be regulated similarly and identified common *cis*-regulatory motifs in genes belonging to the same cluster. This strongly suggested that transcription factor bias for a particular motif regulated the dynamics of transcript expression.

Our 271 transcriptional dynamics were grouped based on their similarity to one another using the MATLAB k-means algorithm. The initial cluster centroid was chosen randomly, and the distance metric which was minimized was the euclidean distance between the sample points and the cluster centroid (Figure 5.2). The algorithm was iterated until the distance metric was minimized. To determine the appropriate number of clusters, we used the elbow method (Figure 5.3). In other words, the algorithm was run for increasing number of clusters and the number of clusters was plotted versus the distance. The point at which this curve forms an "elbow" is the point at which the distance between the data and the model no longer appreciably falls with each added cluster. After the elbow, newly added centroids cluster transcriptional trajectories based on small differences or

experimental noise and fail to convey new features of the dynamics.

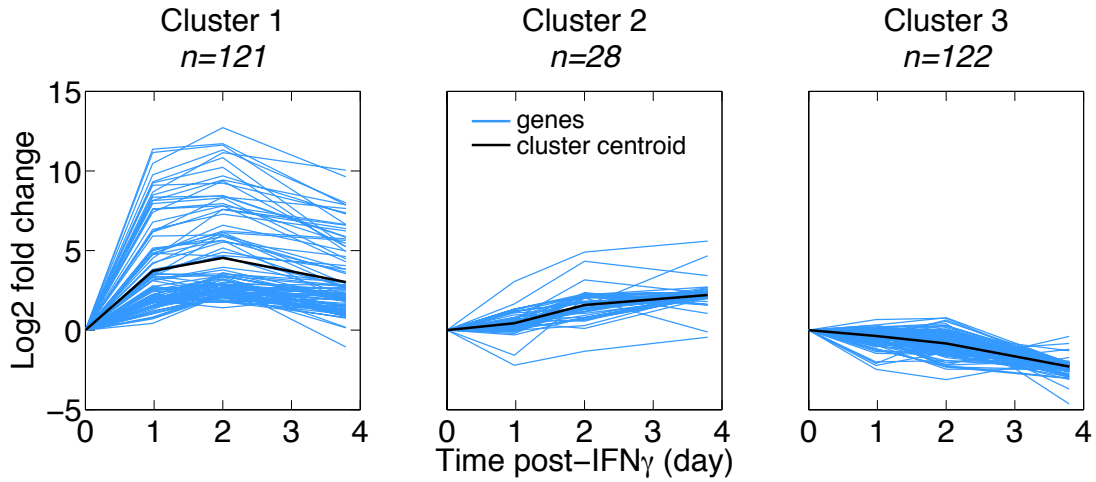

Figure 5.2: **Clustering of transcript dynamics reveals 3 classes of transcription.** Genes were clustered using the k-means algorithm. Each line represents the mean of duplicate RNA samples.

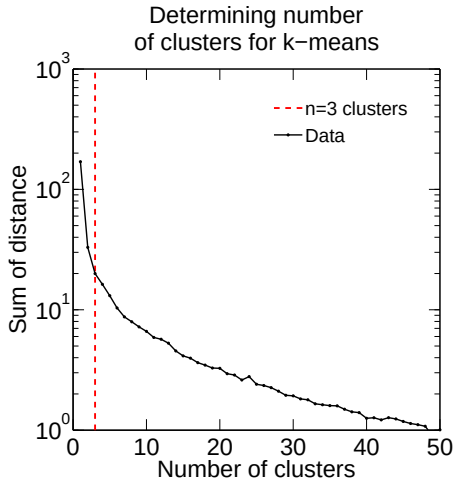

Figure 5.3: **The elbow method for determining number of clusters.** The k-means algorithm was run for increasing number of clusters (n=1-50).

We chose the two candidate genes from cluster 1, H2-D^b and H2-K^b, which encode both haplotypes of mouse MHC-I, to confirm that protein expression matched that of mRNA expression (Figure 5.4). B16 cells were pulsed with 10nM IFNγ, washed, and cultured in fresh media. To quantify protein, cells were harvested at

the indicated timepoints, stained for both MHC-I haplotypes (H2-K^b and H2-D^b), and fluorescence was quantified by flow cytometry.

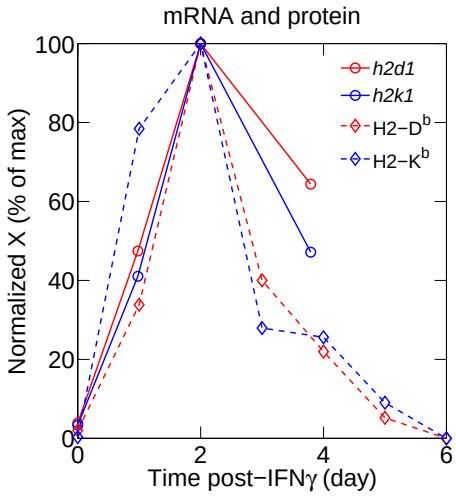

Figure 5.4: **The dynamics of MHC-I protein expression match those of mRNA.** Expression of both MHC-I haplotypes was quantified by flow cytometry and plotted along with the time dynamics of each proteins' corresponding transcript from sequencing data. For both protein and mRNA, data is representative of at least 3 independent experiments.

CHAPTER 6

CHARACTERIZING THE GENE EXPRESSION SIGNATURE OF MELANOMA CELLS FOLLOWING TRANSIENT EXPOSURE TO IFNγ.

Clustering of the mRNA dynamics enabled identification of three main transcriptional classes. Gene ontology analysis [5, 25] was performed on each cluster to identify significantly enriched biological pathways (Figure 6.1). Cluster 1 was significantly enriched with genes involved in the MHC-I and II antigen presentation pathways, which are critical for T cell activation. Furthermore, these genes exhibited a pattern of expression very similar to that of T cell activation. From here on, we will refer to this cluster as the antigen presentation cluster. In Cluster 2, there were no significantly enriched biological pathways. Cluster three was modestly enriched with genes involved in cell cycling, however, since cell cycle genes are not typically associated with T cell activation, we focused on cluster 1. Specifically, we asked what molecular mechanism extends the cells' transcriptional response in the absence of the original signal.

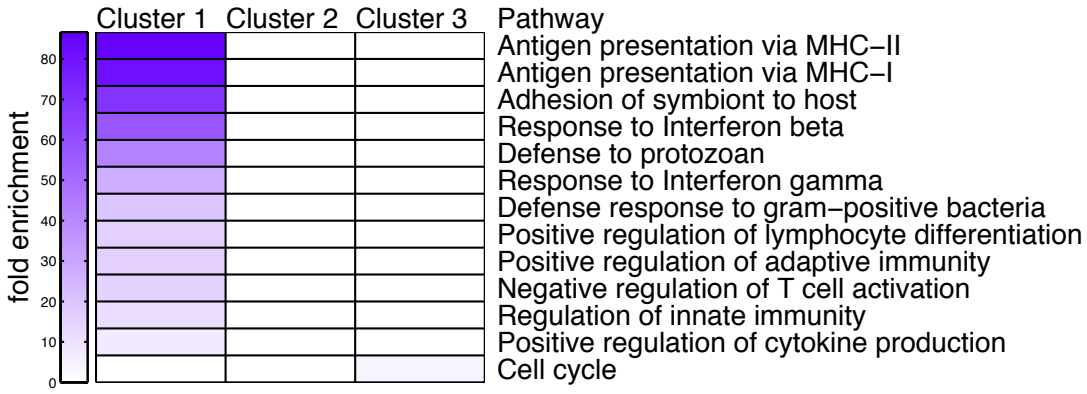

Figure 6.1: **GO analysis reveals enrichment for the class I and II antigen presentation pathway.** Gene ontology analysis was performed for genes in each cluster. Every pathway that was significantly enriched with a p-value < 0.05 was kept and plotted.

6.1 Summary

To summarize data from the previous sections, our *in vitro* assay established that B16 melanoma cells respond to transient IFNγ (5h) with sustained up-regulation of genes in the antigen presentation pathway that peak in expression 2 days post-exposure. Thus, the cell response to IFNγ extends long past the time when the original cytokine is gone. This persistent up-regulation of antigen presentation genes is functionally important, because it controlled T cell activation. The remainder of the dissertation will be devoted to uncovering the molecular mechanism responsible for persistent transcription of IFNγ-response genes.

CHAPTER 7

IDENTIFYING THE MOLECULAR MECHANISM(S) THAT REGULATE THE TEMPORAL DURATION OF THE MELANOMA RESPONSE TO TRANSIENT IFNγ.

7.1 JAK-STAT signaling drives persistent transcription

We asked what mechanism drives the long-term pattern of gene expression we observed in response to transient IFNγ. Downstream of the IFNγ receptor, the transcription factor STAT1 is phosphorylated (pSTAT1) and drives gene expression changes. If STAT1 is persistently phosphorylated after IFNγ withdrawal, it could drive persistent up-regulation of antigen presentation genes. We tested this experimentally by exposing cells to IFNγ for several hours, followed by thorough washing (Figure 7.1a). Cells were harvested periodically for intracellular phosphoflow cytometry of pSTAT1. After stimulation with IFNγ, pSTAT1 peaks rapidly, and decays to about 10% of the maximum after washing (Figure 7.1b). Phosphorylated STAT1 then increases to 20% of its maximum one day later, before slowly decaying back to baseline four days after the initial exposure.

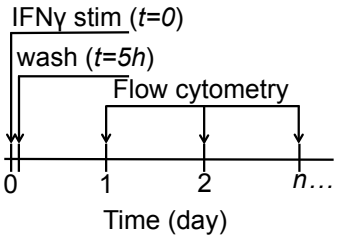

(a) **Diagram of pSTAT1 experiment setup.** B16 cells were pulsed for 5h with 10nM IFNγ, then washed. At indicated timepoints cells were rapidly fixed, permeabilized, then stained. pSTAT1 was quantified by flow cytometry.

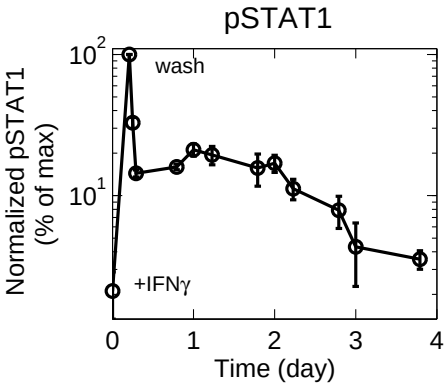

(b) **STAT1 persists long after removal of IFNγ.** Data plotted is the mean and s.e.m. (errorbars) and representative of 2 independent experiments.

Figure 7.1: Phosphorylation of STAT1 persists long after removal of IFNγ.

Persistent phosphorylation of STAT1 requires JAK activity, because application of a JAK inhibitor after IFNγ-stimulation caused rapid decay of pSTAT1 signaling (Figure 3.2b). We checked whether JAK-STAT signaling is necessary for persistent transcription of antigen presentation genes by applying a JAK inhibitor to cells and quantifying *h2kb* transcript over time (Figure 7.2a). Cells that were JAK inhibited after IFNγ-stimulation peaked at five hours, which was the time when JAK inhibitor was applied to cells (Figure 7.2b). Taken together, these data show that after washing, pSTAT1 does not rapidly return to its baseline level, instead, STAT1 is persistently phosphorylated for several days. In addition, this persistent JAK-STAT signaling is necessary for continued transcription of antigen presentation genes.

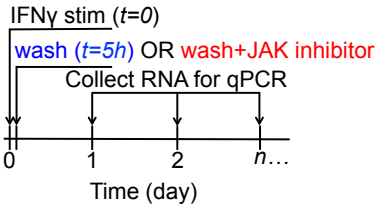

(a) **Diagram of JAKi experiment.** B16 cells were pulsed for 5h with 10nM IFNγ, then washed. Alternatively, washed cells were exposed to 10μM of the JAK inhibitor AZD1480. At indicated timepoints cells RNA was harvested and *h2kb* transcript was quantified by RT-qPCR.

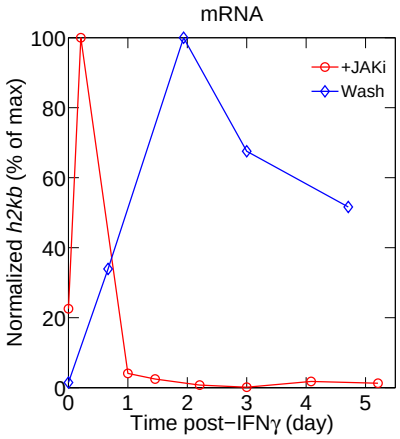

(b) **Persistent MHC-I transcription is JAK-STAT-dependent.** Data plotted is representative of 2 independent experiments.

Figure 7.2: Persistent transcription of *h2kb* is JAK-STAT-dependent

Persistent JAK-STAT signaling could be explained by positive feedback induced through α, β, or γ interferon. IFNα/β are induced in response to stimulation with IFNγ, albeit at low levels, and also signal through STAT1 [1, 73]. However, neither α nor β interferons drove persistent up-regulation of the antigen presentation pathway (Figure 7.3).

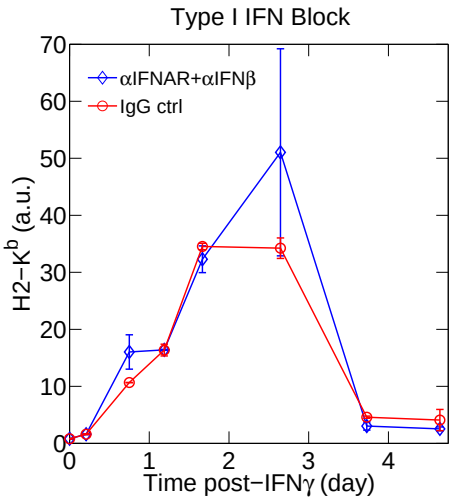

Figure 7.3: **Type I Interferons do not drive persistent up-regulation of antigen presentation genes.** Cells were stimulated with 10nM IFNγ, then washed. At the time of wash, one cohort of cells received neutralizing antibodies directed against both the common receptor for IFNα/β and the cytokine IFNβ. The other cohort received IgG control antibodies. MHC-I was measured by flow cytometry. Data plotted is the mean and s.e.m. (errorbars) and representative of 3 independent experiments.

To test whether IFNγ drives persistent gene up-regulation, we stimulated cells with cytokine for several hours, washed, and added a neutralizing antibody directed against soluble IFNγ (Figure 7.4a). Indeed, extracellular blocking of IFNγ after the initial washout caused an early peak in the MHC-I protein H2-K^b relative to the control (Figure 7.4b).

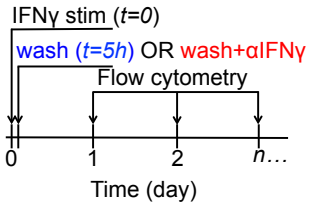

(a) **Diagram of αIFNγ experiment.** B16 cells were pulsed with 10nM IFNγ, then washed. At the time of wash one cohort of cells received neutralizing antibodies directed against IFNγ. MHC-I was measured by flow cytometry.

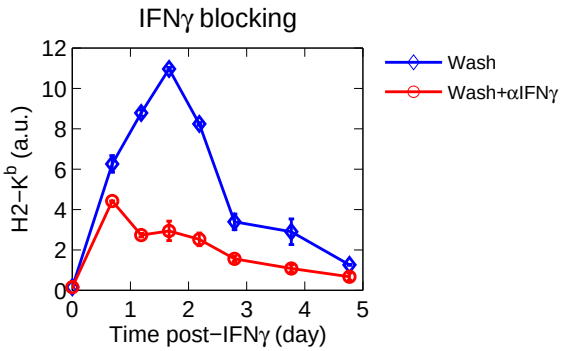

(b) **Persistent transcription is IFNγ-dependent.** Data plotted is the mean and s.e.m. (errorbars) and representative of 3 independent experiments.

Figure 7.4: Persistent up-regulation of antigen presentation genes is IFNγ-dependent

We estimated that the washing we perform after IFNγ exposure amounts to an approximate billion-fold dilution of the original IFNγ concentration. Specifically, after a 5h culture with IFNγ, cells are centrifuged, then washed three consecutive times with a large volume (10mL) of warm culture media. However, we confirmed that conditioned media harvested immediately after the last wash does not cause up-regulation of antigen presentation genes when cultured with naive B16 cells (Figure 7.5). To confirm this, B16 cells were pulsed for 5h with 10nM IFNγ, then washed. Immediately after the last wash, the conditioned media was harvested from the B16 cells. Next, a fresh, unstimulated cohort of cells were stimulated with either media alone, 10nM IFNγ, or conditioned media. MHC-I was measured by flow cytometry after 1 day of culture. Since IFNγ-pulsed cells were only exposed to the conditioned media for an approximate 3 minute wash, any up-regulation of MHC-I in response to the conditioned media could be attributed to residual IFNγ remaining in the media caused by insufficient washing.

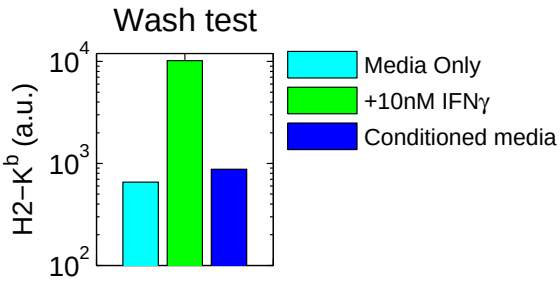

Figure 7.5: **Persistent transcription of antigen presentation genes is not caused by insufficient washout of IFNγ.** B16 cells were pulsed for 5h with 10nM IFNγ, then washed. Immediately after the last wash, conditioned media was harvested. A fresh cohort of cells were cultured in either conditioned media, 10nM IFNγ, or media alone for 1 day. MHC-I was quantified by flow cytometry.

Given that an IFNγ antibody blockade prevents sustained up-regulation of IFNγ response genes, we hypothesized that IFNγ induces its own production via a positive feedback loop. However, when we checked our sequencing data, we did not observe induction of the *ifng* gene, suggesting the cytokine originates from cells in a manner independent of transcription. In summary, IFNγ drives persistent JAK-STAT signaling, which causes persistent up-regulation of the antigen presentation pathway. However, cells do not transcribe IFNγ.

7.2 IFNγ-exposed cells release cytokine with very slow kinetics

We next asked whether IFNγ originates from cytokine-pulsed cells. To test this, we set up a transwell assay (Figure 7.6a). In this assay, one group of cells were stimulated with IFNγ, washed, and co-cultured in the bottom of a plate with naive, un-stimulated sensor cells. We distinguished between the two groups by labeling sensor cells with a fluorescent dye. An additional group of un-stimulated

sensor cells were spatially separated from cytokine-pulsed sharing cells by placing them in the top of a 0.4μm pore diameter transwell insert. This pore size allows molecules, but not cells to freely pass across. MHC-I on sensor cells was measured by flow cytometry after one day of co-culture. We reasoned that if IFNγ originates from pulsed cells, only sensor cells cultured in the bottom of the plate (in close proximity) with pulsed cells would up-regulate MHC-I at this timepoint. To ensure that any effects we observed were dependent on IFNγ, an additional well received IFNγ neutralizing antibodies.

Our results validated our hypothesis that IFNγ originates from cytokine-pulsed cells. Sensor cells cultured in close proximity with IFNγ-pulsed cells up-regulated MHC-I approximately 10-fold after 1 day of co-culture (Figure 7.6b). However, sensor cells cultured in the top of the transwell or in close proximity with IFNγ-pulsed cells, but with IFNγ neutralizing antibodies did not up-regulate MHC-I.

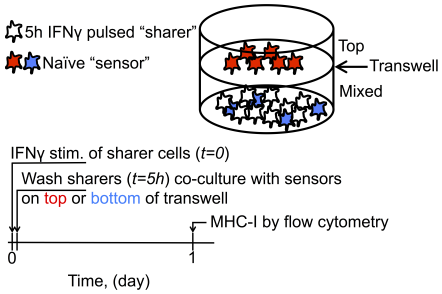

(a) **Cartoon diagram of transwell experiment.** One group of cells were pulsed with 10nM IFNγ for 5h, then washed. Cytokine-pulsed cells were co-cultured in the bottom of of a transwell with fluorescent-labeled, naive, unpulsed sensor cells. An additional group of sensor cells were cultured on the top of a transwell insert that is permeable to small molecules, but not cells. As a control, an additional well received neutralizing antibodies directed against IFNγ.

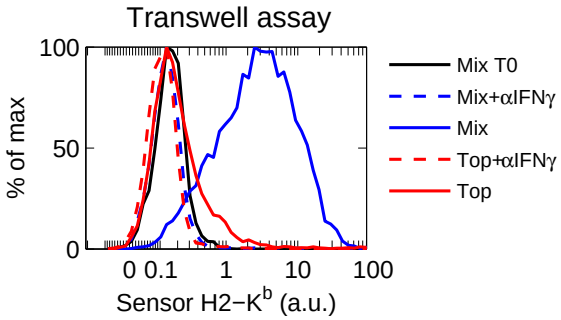

(b) **IFNγ originates from cytokine-pulsed cells.** MHC-I was measured by flow cytometry after 1 day of co-culture. Experiment is representative of at least 3 independent experiments.

Figure 7.6: IFNγ originates from cytokine-pulsed cells.

To determine whether cell-to-cell cytokine sharing is dependent on cell proximity or cell contact, we measured MHC-I expression on sensor cells in the top and bottom of the transwell after multiple days of co-culture. After several days, sensor cells mixed in the bottom of the transwell continued to up-regulate MHC-I, and sensor cells in the top of transwell began to up-regulate MHC-I, eventually reaching levels comparable to mixed sensor cells (Figure 7.7). This suggested that IFNγ is slowly released from IFNγ-pulsed sharing cells and diffuses up to sensor cells in the top of the transwell over time. Thus, cell-to-cell cytokine sharing likely depends on proximity (due to diffusion), but not cell contact.

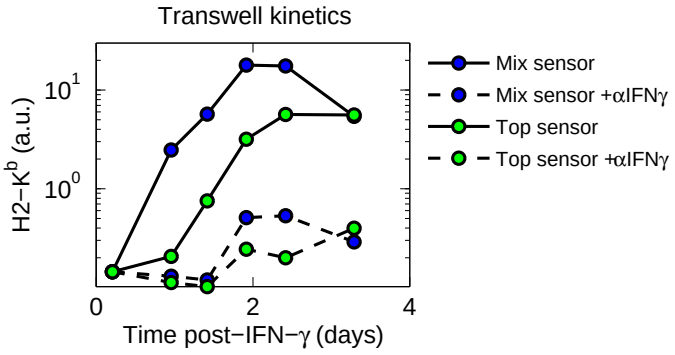

Figure 7.7: **Cell-to-cell cytokine sharing is proximity, but not contact-dependent.** The transwell assay was repeated and timepoints were taken for several days. MHC-I was measured by flow cytometry.

We then asked whether other cell types exhibit cell-to-cell cytokine sharing. A panel of mouse and human cells were pulsed with mouse IFNγ, then washed and co-cultured with naive, unstimulated B16 sensor cells (Figure 7.8a). Specifically, B16 mouse melanoma, Mel-2 human melanoma, H460 human lung carcinoma, CH12 mouse B cell lymphoma, Hek293T human embryonic kidney, and RAW mouse macrophages were all pulsed with 10nM mouse IFNγ for 5h, washed, and co-cultured with naive, unstimulated B16 sensor cells. MHC-I was measured on B16 sensor cells as a readout of cell-to-cell cytokine sharing. The strength of

this experiment is that cell-to-cell cytokine sharing can be compared across cell lines because only one cell type (B16) reads out the response. If we had used different sensor cells, variable responsiveness to IFNγ could confound comparison between groups. All cell types assayed, including tumor- and non-tumor derived, were capable of sharing IFNγ with B16 cells (Figure 7.8b). These experiments demonstrated that IFNγ can be captured by diverse cell types and then slowly released over long timescales to signal in a manner dependent on cell proximity, but not contact. In addition, these results indicated that the mechanism of IFNγ capture by cells is not species-specific.

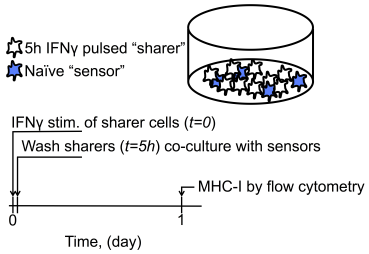

(a) **Cartoon diagram of sensor/sharer experiment.** This experimental design applies generally to several of the following experiments. One group of cells were first pulsed with 10nM IFNγ, then washed and co-cultured with another group of fluorescently-labeled, naive, unstimulated sensor cells. MHC-I on sensor cells was measured by flow cytometry after 1 day of co-culture.As a control, an additional well received neutralizing antibodies directed against IFNγ.

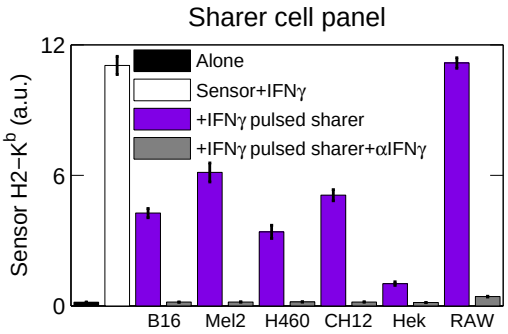

(b) **IFNγ can be shared by diverse cell types.** A panel of diverse, tumor- and non-tumor-derived human and mouse cell lines were pulsed for 5h with 10nM mouse IFNγ, then washed and co-cultured with naive, unstimulated B16 sensor cells. MHC-I was measured by flow cytometry after 1 day of co-culture. Data plotted are mean and s.e.m. (errorbars).

Figure 7.8: Cell-to-cell cytokine sharing is observed in diverse cell types.

We also checked whether human IFNγ can participate in cell-to-cell cytokine sharing. Human H460 lung carcinoma cells and Mel-2 human melanoma cells were pulsed with 10nM human IFNγ for 5h, then washed and co-cultured with naive, unstimulated H460 or Mel-2 as sensor cells. Expression of Human Leukocyte Antigen

A/B (HLA-A/B) was quantified by flow cytometry after 24h of co-culture. Indeed, human IFNγ can also participate in cell-to-cell cytokine sharing (Figure 7.9). Notably, the degree of HLA up-regulation was much lower in these human cell lines when compared to B16. This illustrates the degree of cell type-to-cell type variability in responsiveness to IFNγ.

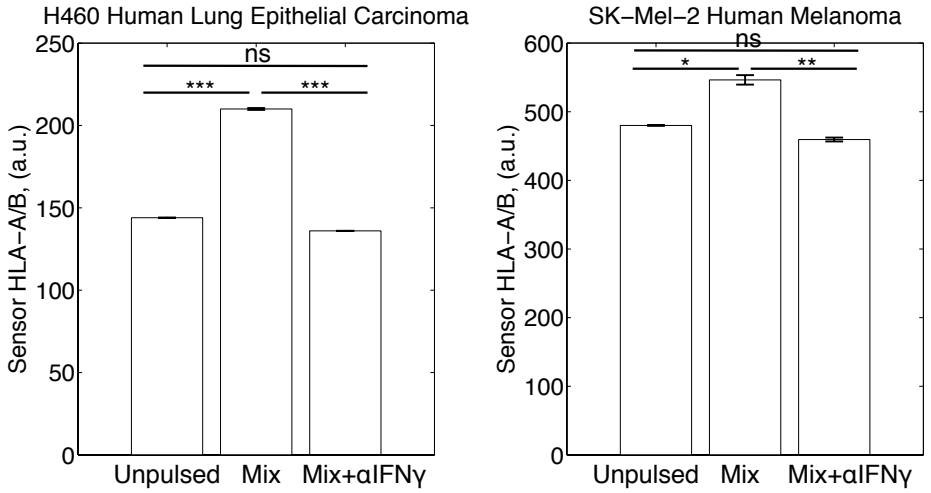

Figure 7.9: **Human IFNγ also participates in cell-to-cell cytokine sharing.** H460 or Mel-2 human cells were pulsed with 10nM human IFNγ, washed, and co-cultured with naive, unstimulated cells as sensors. Expression of HLA-A/B was quantified by flow cytometry as a readout of cell-to-cell cytokine sharing. The data plotted are mean and s.e.m (errorbars) and representative of 2 independent experiments. Statistical significance was computed using an unpaired T test.

We next addressed whether IFNγ de-binds from IFNγ receptors after washing to mediate signaling. Based on our previous results, this would imply that mouse IFNγ can at least bind to both the human and mouse IFNγ receptor. To test this, we repeated our assay with B16 IFNγ receptor knockout (B16 IFNγR KO) cells. These cells were pulsed with IFNγ, washed, and co-cultured with receptor competent B16 sensor cells (Figure 7.8a). We again observed IFNγ-dependent up-regulation of MHC-I on sensor cells despite lack of the IFNγ receptor on IFNγ-pulsed cells (Figure 7.10a). This showed that IFNγ associates with cells in a

receptor-independent manner.

Finally, we repeated this assay with a stringent wash. We pulsed B16 IFNγR KO cells with IFNγ for 5h, then washed them. Cells were then briefly exposed to a low-pH solution at 4°C. This acid-stripping has been shown to remove all non-covalently bound molecules from cell surfaces [17]. Acid-stripped cells were then co-cultured with B16 sensor cells. We found that acid-stripping knocked down the ability of IFNγ-exposed sharer cells to induce MHC-I up-regulation, but did not completely eliminate it (Figure 7.10b). MHC-I up-regulation on sensor cells was reduced by approximately 5-fold when sensors were co-cultured with acid-stripped cells. This suggests that some of the shared IFNγ is present on the cell surface while an additional fraction remains inside the cells.

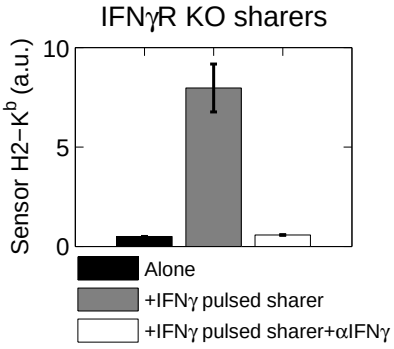

(a) **Cell-to-cell cytokine sharing is mediated by IFNγ de-binding from the IFNγR.** B16 IFNγR KO cells were stimulated with 10nM IFNγ for 5h, then washed and co-cultured with naive, unstimulated, receptor-competent B16 sensor cells. MHC-I on sensor cells was measured by flow cytometry after 1 day of co-culture. As a control, an additional well received neutralizing antibodies directed against IFNγ. Data plotted is mean and s.e.m. (errorbars) and representative of at least 3 independent experiments.

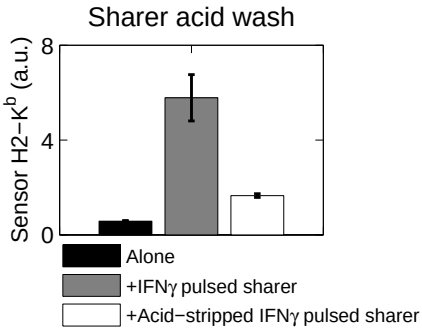

(b) **Some IFNγ is internal and some is surface-exposed.** B16 IFNγR KO cells were pulsed with 10nM IFNγ for 5h, then washed. After washing, one cohort of cells was washed with stripping buffer (0.25M glycine, 0.125M NaCl, pH 4.0) [17]. This acid-strip wash removes everything that is non-covalently bound to the cell surface. Cells were then cultured with naive, unstimulated, receptor-competent B16 sensor cells. MHC-I on sensor cells was measured by flow cytometry after 1 day of co-culture. Data plotted is mean and s.e.m. (errorbars) and representative of 2 independent experiments.

Figure 7.10: IFNγ is both intracellular and surface-exposed, and its release is independent of the IFNγR

IFNγ produced by activated primary T cells is known to undergo post-translational modifications [22], so we wanted to verify that both T cell-derived and recombinant IFNγ associate with cells. To this end, we developed a quantitative IFNγ cell capture assay (Figure 7.11). B16 IFNγR KO cells were pulsed with 50pM T cell-derived or recombinant IFNγ in a well-mixed setting for several hours. The culture media was then harvested from cells and a bead-based ELISA was used to quantify the depletion of IFNγ from the media. We confirmed that both T cell-derived and recombinant IFNγ could be captured equivalently by IFNγR KO cells (Figure 7.12).

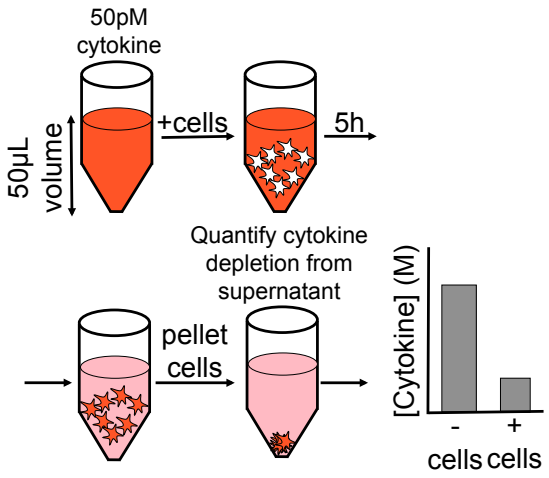

Figure 7.11: **Cartoon diagram of cytokine capture assay.** B16 IFNγR KO cells were pulsed with 50pM cytokine in 50μL total volume in a well-mixed setting for several hours. The culture media was then harvested from cells and a bead-based ELISA was used to quantify the depletion of IFNγ from the media. A standard curve was used to convert bead fluorescence into cytokine molarity. Molarity was then converted into number of molecules per tube. The amount of cell-based capture was quantified by taking the difference between the number of molecules in the cell free condition and the number of molecules in the conditions with added cells.

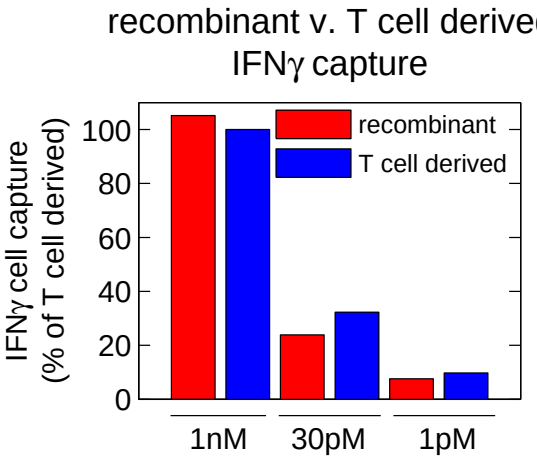

Figure 7.12: **Recombinant and T cell-derived IFNγ associate with cells equally well.** B16 IFNγR KO cells were pulsed with 50pM T cell-derived or recombinant IFNγ in a well-mixed setting for several hours. The culture media was then harvested from cells and a bead-based ELISA was used to quantify the depletion of IFNγ from the media.

To summarize this section, IFNγ can be captured by cells, exists primarily on the membrane or is at least accessible to acid-based removal, and is released slowly to signal to neighboring cells in a proximity-dependent manner.

7.3 IFNγ cell capture is cholesterol-dependent

We then sought to identify what surface molecule would achieve this slow catch-and-release. IFNγ has been shown to associate electrostatically with peri-cellular matrix proteoglycans such as chondroitin sulfate and heparan sulfate [7, 51]. These peri-cellular proteoglycans are fairly ubiquitous across cell lines that form epithelia and grow in monolayers (our own data, not shown). We repeated our IFNγ cell capture assay (Figure 7.11) after enzymatic removal of heparan sulfate and chondroitin sulfate, however, we observed no reduction in IFNγ cell association (Figure 7.13). In addition, treatment of cells with dynasore, an inhibitor of clathrin and dynamin-dependent endocytosis, did not inhibit IFNγ cell capture (Figure 7.13). We next tested whether IFNγ associated with a protein on the cell surface by digesting cell-surface proteins with pronase [83], then performing the IFNγ cell capture assay. Again, there was no reduction in IFNγ cell association despite protein digestion (Figure 7.13). Surprisingly, IFNγR-independent capture of IFNγ on the cell surface did not depend on proteins, clathrin-dependent endocytosis, or proteoglycans.

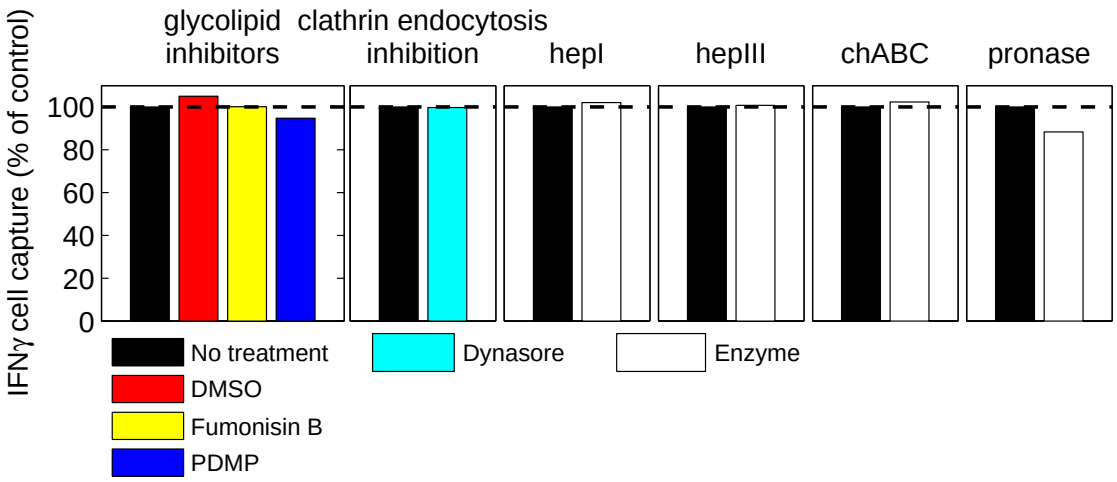

Figure 7.13: **IFNγR-independent capture of IFNγ on the cell surface does not depend on proteins, internalization, or proteoglycans.** B16 IFNγR KO cells were pulsed with 50pM T cell-derived or recombinant IFNγ in a well-mixed setting for two hours. The culture media was then harvested from cells and a bead-based ELISA was used to quantify the depletion of IFNγ from the media. For ganglioside depletion, cells were treated with 10μM of either Fumonisin B1 or PDMP (N-[2-hydroxy-1-(4-morpholinylmethyl)-2-phenylethyl]-decanamide, monohydrochloride), or DMSO as a vehicle control for 3 days prior to performing the capture assay [70]. To block clathrin and dynamin-dependent endocytosis, cells were treated with 30μM dynasore for 1h prior to performing the capture assay. To digest cell surface proteoglycans, cells were treated with 5U/mL either heparinase I, III, or chondroitin ABC lyase 1h prior to performing the assay. To digest proteins, cells were treated with 0.01% pronase for 30 minutes prior to performing the assay [83].

To get a clue about what cell surface molecule IFNγ could bind to, we generated fluorescently-tagged IFNγ (IFNγ-A647 and IFNγ-A488). This enabled us to visualize the spatial distribution of IFNγ when captured by the cell. To ensure that our fluorescently-tagged IFNγ behaved like recombinant, unlabeled IFNγ, we performed a panel of control experiments (Figure 7.14).

First, we confirmed that fluorescent IFNγ could be captured by cells on a population wide scale (black). Second, we confirmed that residual dye left in the prep could not bind cells, potentially resulting in false positive staining (red). Third,

we confirmed that the binding of IFNγ-A647 to cells is specific by pre-incubating cells with unlabeled IFNγ before IFNγ-A647 (cyan). This treatment did result in an increase in cell fluorescence, however, based on simple binding-debinding, we would assume that after several hours of culture with equimolar concentrations of unlabeled IFNγ and IFNγ-A647, there would be some replacement of the unlabled IFNγ. The observation that pre-treatment with unlabeled IFNγ strongly reduces the cell fluorescence relative to the untreated control indicates that the binding is specific. Finally, we checked whether IFNγ-A647 could be partially stripped from cells by treatment with low pH glycine buffer, similar to unlabeled IFNγ in (Figure 7.10b) (blue). In (Figure 7.10b), acid stripping of cells pulsed with unlabeled IFNγ resulted in a 5-fold reduction in sensor cell MHC-I expression. Similar to this result, acid stripping of fluorescently-tagged IFNγ reduced cell fluorescence by 5-fold. This result suggests that some of the IFNγ is protected from acid treatment possibly due to an intracellular location. Taken together, these controls suggest that fluorescently-tagged IFNγ behaves similarly to unlabeled IFNγ.

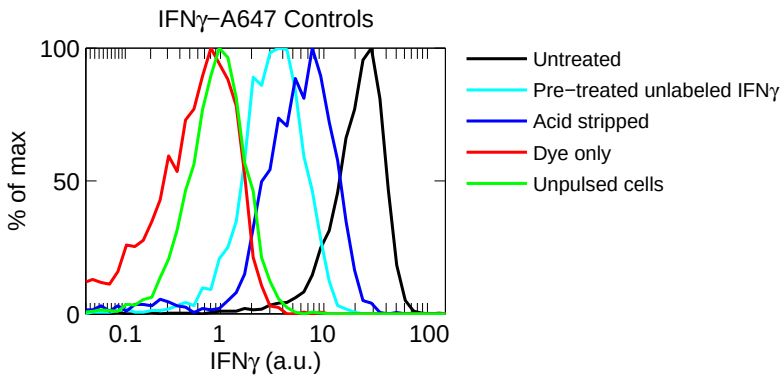

Figure 7.14: **Association of IFNγ-A647 with cells is specific.** B16 IFNγR KO cells were pulsed for 3.5 hours with 10nM IFNγ-A647 while tumbling in RPMI, then washed (black). To acid strip, cells treated with IFNγ-A647 were first washed once in cold PBS, then exposed to glycine stripping buffer (0.25M glycine, 0.125M NaCl, pH 4.0) for 2 minutes on ice. Cells were then rapidly pelleted, washed once in cold FACS buffer, and kept on ice. To pre-treat cells with unlabeled IFNγ, cells were pre-treated with 10nM IFNγ for 3.5 hours after which 10nM IFNγ-A647 was spiked in for an additional 3.5 hours. To assess the potential non-specific binding or uptake of dye particles left in the prep, we prepared a protein-free sample of Alexa647 carboxylic acid succinimidyl ester dye treated exactly as the IFNγ-A647 was treated and exposed an equal quantity to cells for 3.5 hours. Data are representative of 2 independent experiments.

In addition, we confirmed that fluorescent IFNγ is functionally equivalent to unlabeled, recombinant IFNγ (Figure 7.15). B16 IFNγR KO cells were pulsed with 10nM either fluorescent or unlabeled IFNγ for 5h then washed. Washed cells were co-cultured with unstimulated sensor cells for 24 hours. αIFNγ was added to relevant wells to block IFNγ signaling.

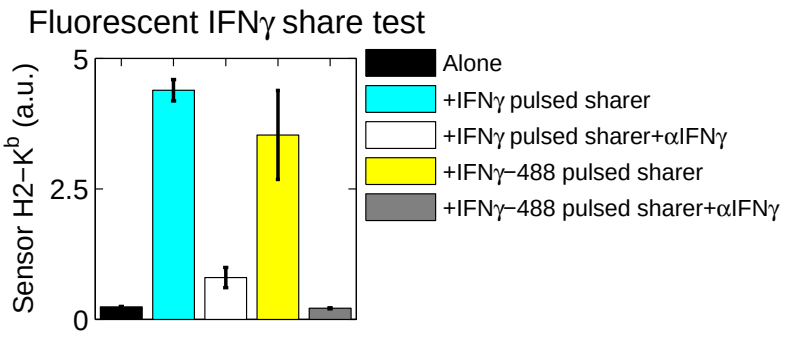

Figure 7.15: **Fluorescent IFNγ is functionally equivalent to unlabeled IFNγ.** B16 IFNγR KO cells were pulsed with 10nM either fluorescent or unlabeled IFNγ for 5h then washed. Washed cells were co-cultured with unstimulated sensor cells for 24 hours. αIFNγ was added to relevant wells to block IFNγ signaling. MHC-I was measured after 1 day of co-culture. Data plotted are mean and s.e.m. (errorbars).

Cells were then imaged using confocal microscopy. B16 IFNγR KO cells were adhered to the surface of fibronectin-coated glass-bottom culture plates, then pulsed for several hours with 10nM IFNγ-A4647. Cells were washed with phenol-free RPMI and imaged. Imaging revealed that IFNγ assumed a punctate pattern on cells, and this morphology resembled membrane lipid micro-domains (Figure 7.16) [24].

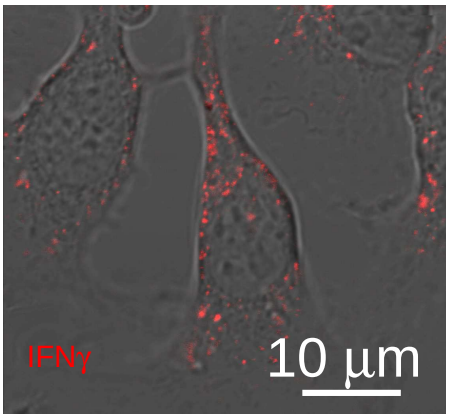

Figure 7.16: **IFNγ assumes a punctate distribution on cells.** B16 IFNγR KO cells were adhered to fibronectin-coated glass bottom dishes and incubated with 10nM IFNγ-A647 for several hours, then washed and imaged via confocal microscopy. Imaging is representative of at least 3 independent experiments.

Earlier, we showed that acid-stripped IFNγ-pulsed cells exhibit reduced cell-to-cell cytokine sharing (Figure 7.10b). In addition, acid-stripping reduced IFNγ cell fluorescence by about 5-fold when cells had been pulsed with IFNγ-A647 (Figure 7.14). These results suggested that there are pools of intracellular and surface-accessible IFNγ. To check this, we analyzed the intracellular versus cell surface-bound fractions of IFNγ by confocal microscopy. When cells were flattened and adhered to glass coverslips, it was difficult to resolve whether IFNγ is intracellular or surface-exposed (Figure 7.16). To circumvent this problem, we pulsed B16 IFNγR KO cells with 10nM IFNγ-A488 for 5 hours, washed them, stained the cell membrane with the dye Cell Mask Orange, deposited them on untreated glass slides, and imaged immediately. Using this strategy the cells remained round and it was easier to see the subcellular localization of the cytokine based on its position relative to the cell membrane dye.

We pseudo-colored IFNγ green and cell mask orange red. This way, we could conclude that yellow color represented co-localization between the cytokine and the plasma membrane. From this imaging, it was clear that much of the IFNγ was co-localized with the cell membrane, resulting in a yellow color (Figure 7.17a). Much of the remaining IFNγ appeared to be just adjacent to or underneath the cell membrane (Figure 7.17b).

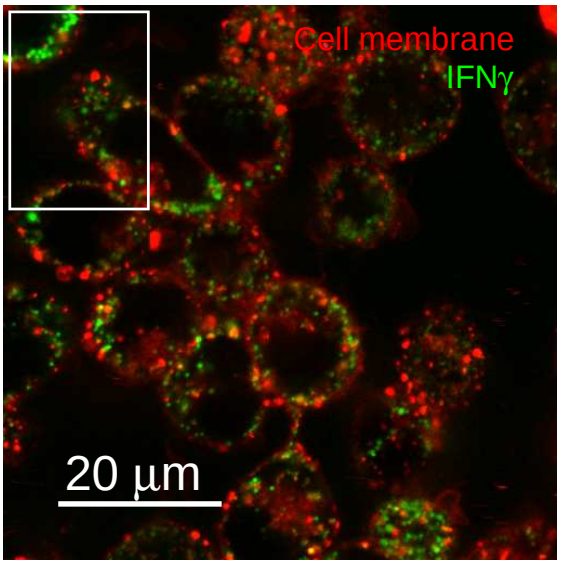

(a) **Imaging the subcellular localization of IFNγ.** B16 IFNγR KO cells were stimulated with 10nM IFNγ-A488 for 5 hours, then washed. Washed cells were then stained with Cell Mask Orange, which labels the plasma membrane, then deposited and imaged immediately on untreated glass slides. Image is representative of 2 independent experiments.

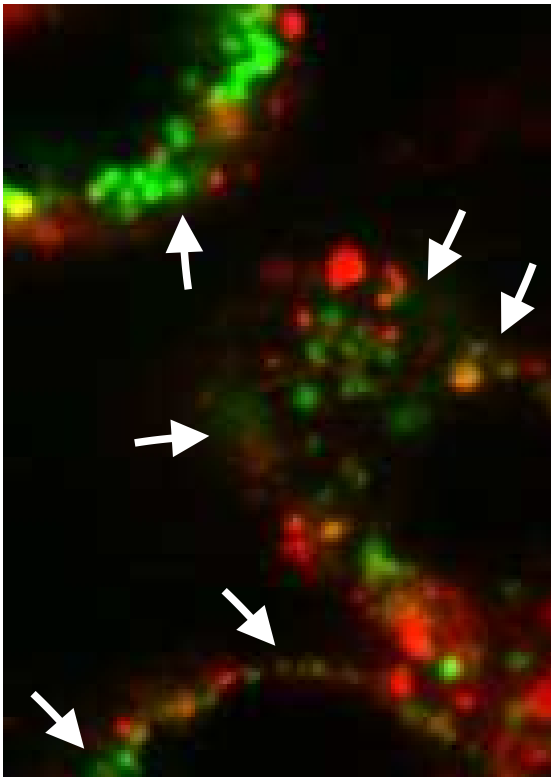

(b) **Close-up shows surface-exposed IFNγ.** This picture shows a close-up of the boxed image in A. The arrows show examples of surface-exposed or plasma membrane-bound IFNγ. (yellow = co-localized IFNγ and plasma membrane)

Figure 7.17: IFNγ is both intracellular and surface-exposed.

We also sought to interrogate the IFNγ distribution after treatment with low pH. In parallel, an additional cohort of IFNγ-A488-pulsed cells were exposed to acidic stripping buffer for 2 minutes on ice, then washed. Cells were rapidly stained with Cell Mask Orange and deposited onto untreated glass slides for imaging. Images of acid-stripped and un-treated cells were acquired using identical microscope settings. Both sets of images were processed by removing the bottom 2% of red pixels (to reduce background). Visual examination of these images revealed that IFNγ fluorescence decreases markedly after acid strip treatment (Figure 7.18a).

When focusing on a single cell, it was clear that the only remaining IFNγ is deep inside the cell. All membrane-bound IFNγ and IFNγ situated just under the membrane is effectively removed (Figure 7.18b).

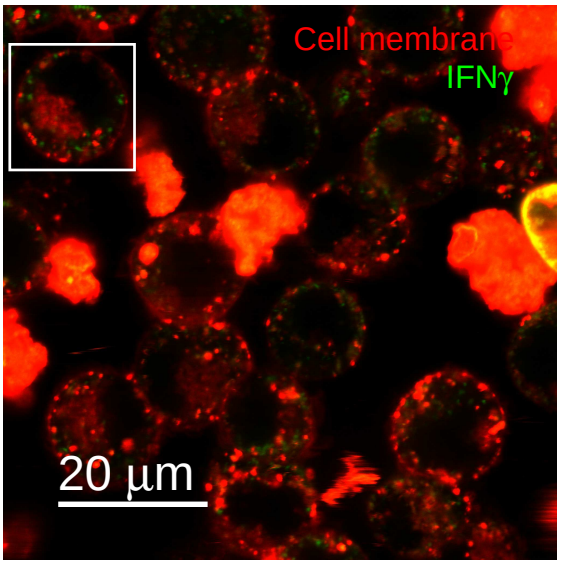

(a) **Imaging the subcellular localization of IFNγ after acid stripping.** B16 IFNγR KO cells were stimulated with 10nM IFNγ-A488 for 5 hours, then washed. Cells were then acid stripped by first washing cells in PBS, then exposing to acidic stripping buffer for 2 minutes on ice. Cells were then rapidly stained with Cell Mask Orange, which labels the plasma membrane, then deposited and imaged immediately on untreated glass slides.

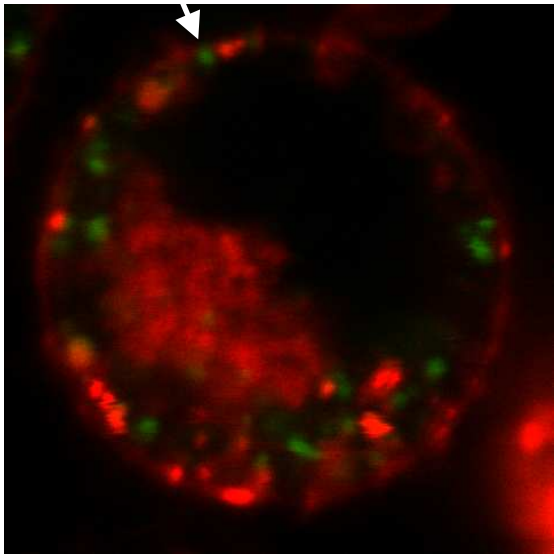

(b) **Close-up shows surface-exposed IFNγ after acid stripping.** This picture shows a close-up of the boxed image in A. The arrows show an example of surface-exposed or plasma membrane-bound IFNγ.

Figure 7.18: IFNγ is both intracellular and surface-exposed.

Consistent with our visual analysis of the images, quantitative comparison reveals a shift in the fluorescence of the IFNγ green channel following acid-strip treatment, whereas the cell membrane channel is super-imposable (Figure 7.19).

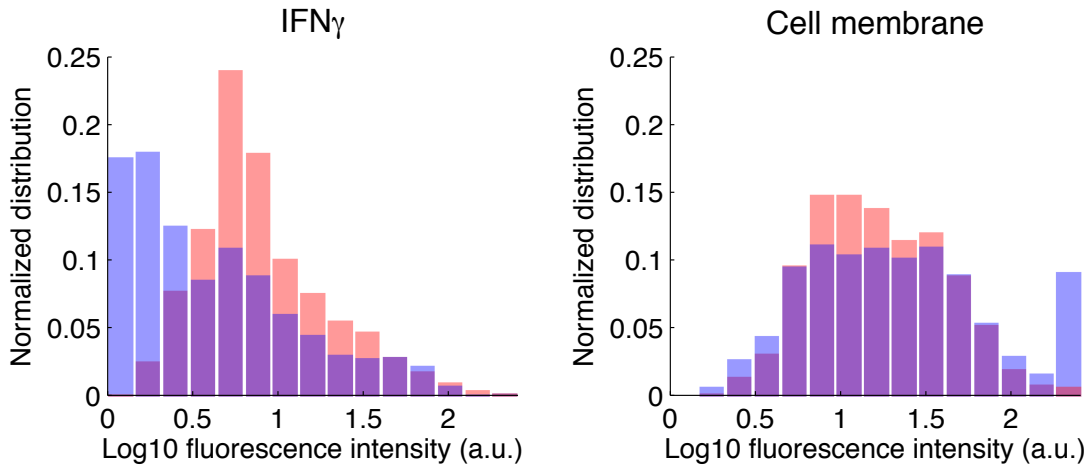

Figure 7.19: **Shift in population-wide IFNγ fluorescence after acid strip.** Images were processed by removing the bottom 2% of red pixels. Histograms show the data from Figure 7.17a and Figure 7.17a

We next tested whether IFNγ co-localized with lipid micro-domains, so we imaged it together with cholesterol, a known component of lipid rafts [24, 80]. We loaded cells with fluorescent topFluor(TF)-cholesterol using the cholesterol donor methyl-β cyclodextrin (MβCD) [36]. TF-cholesterol acts as a cholesterol tracer by partitioning into cholesterol containing cellular compartments. We observed co-localization of cholesterol and IFNγ with a Pearson coefficient of 0.6 (Figure 7.20).

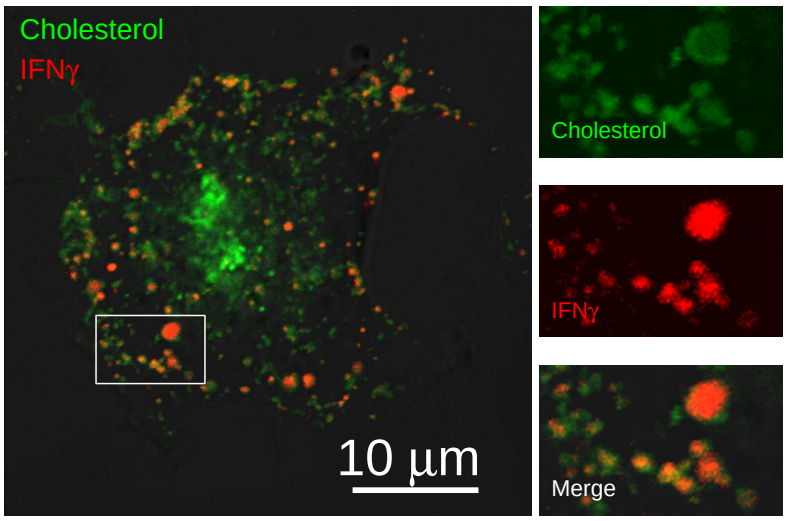

Figure 7.20: **Fluorescent IFNγ co-localizes with cholesterol in lipid microdomains.** First, TF-cholesterol was introduced into B16 IFNγR KO cells. TF-MβCD complexes were mixed in PBS with PBS-washed cells for 5 minutes at 37°C. Cells were then washed in RPMI and adhered to fibronectin-coated glass-bottom culture plates. IFNγ-A647 was then added to cells for several hours. Cells were washed and imaged via confocal microscopy. Imaging is representative of at least 2 independent experiments.

We then asked whether a lipid could be responsible for cell association. The glycolipid ganglioside GM1 occupies lipid micro-domains and is a growth factor co-receptor, so we wondered if it could also bind IFNγ [70]. Ganglioside biosynthesis was inhibited in B16 IFNγR KO cells for one week using two different drugs: Fumonisin B and PDMP (N-[2-hydroxy-1-(4-morpholinylmethyl)-2-phenylethyl]-decanamide, monohydrochloride), before performing our IFNγ cell-capture assay (Figure 7.11). Neither treatment inhibited IFNγ binding (Figure 7.13).This result prompted us to ask whether cholesterol itself is necessary for IFNγ cell association.

When not in complex with cholesterol, MβCD acutely depletes cellular cholesterol [36]. A 40% reduction in IFNγ cell binding was observed when cholesterol was transiently depleted from cells (Figure 7.21). Further confirming this result, pharmacologic inhibition of cholesterol biosynthesis using lovastatin reduced IFNγ

binding by nearly 80%. These data show that cholesterol is both co-localized with IFNγ and necessary for cell capture of the cytokine. In addition, permanent disruption of cholesterol using saponin or filipin also resulted in reduced IFNγ capture. Cholesterol-rich patches on the cell membrane provide an essential scaffolding domain for assembly of caveolins [57]. The observation that cholesterol depletion disrupts cell capture of IFNγ argues for a role of caveolae-dependent internalization of IFNγ, though this has yet to be definitively proven.

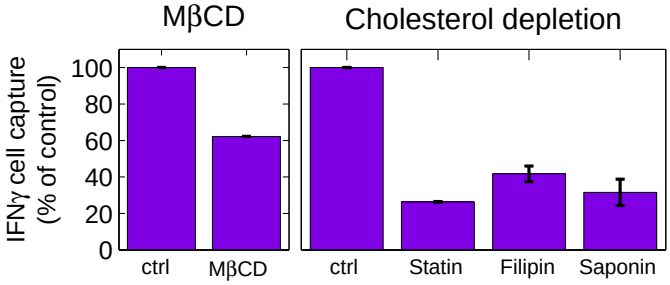

Figure 7.21: **Cholesterol is necessary for IFNγ cell association.** To transiently deplete cholesterol with MβCD, B16 IFNγR KO cells were treated with 10mM MβCD in PBS supplemented with 25mM HEPES buffer for 45 minutes at 37°C. Cells were washed, then the IFNγ cell capture assay was performed. To permanently disrupt cholesterol, cells were treated with 0.1% saponin in RPMI or 50μg/mL filipin in RPMI for 15 minutes prior to performing the IFNγ cell capture assay. To disrupt cholesterol biosynthesis, cells were treated with 10μM lovastatin for 3 days prior to performing the assay. Data plotted are the mean and s.e.m (errorbars) and representative of 3 independent experiments.

To test whether IFNγ directly bound cholesterol, we performed a lipid immunoblot using membranes spotted with cholesterol and a variety of different lipids. Lipid-spotted strips were probed with 50nM IFNγ, and then with IFNγ-specific antibodies. IFNγ did not bind directly to cholesterol, however it did bind to several other lipids (Figure 7.22). These data showed that cholesterol is necessary for IFNγ cell association and possibly internalization, but does not directly bind the cytokine. In addition, they presented several candidate lipids that may mediate cell capture. Interestingly, all of the phospholipids capable of binding

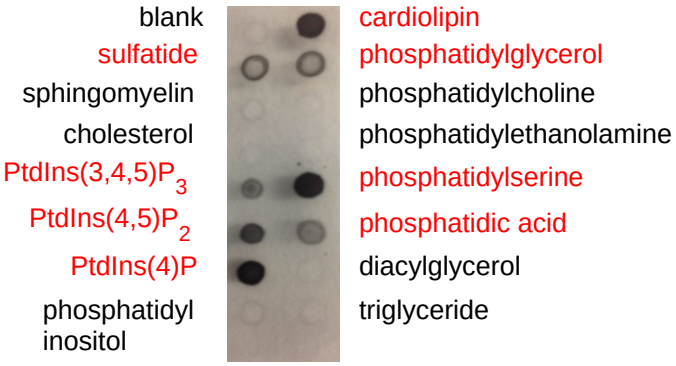

Figure 7.22: **IFNγ does not directly bind cholesterol, but does bind a variety of anionic phospholipids.** Lipid-spotted strips were incubated with 50nM IFNγ, then washed and probed with a primary antibody directed against IFNγ. A secondary HRP-conjugated antibody directed against the primary isotype was then added and blots were developed and visualized. The blot is representative of 3 independently done blots.

IFNγ are anionic, suggesting that the positively charged c-terminal region of IFNγ could mediate binding.

To conclude, we uncovered a cytokine catch-and-release phenomenon, whereby cells exposed to IFNγ capture it on their surface in an IFNγR-independent manner, internalize it, and then release it to neighboring cells. This allows IFNγ to act over long timescales by persisting in the environment after the original signal is gone. We term this mechanism "cytokine catch-and-release communication."

7.4 An updated mathematical model recapitulates experimental results

We wanted to see if our mechanistic understanding of the system could be recapitulated using a mathematical model. In addition, we hypothesized that by using a mathematical model, we could quantitatively interrogate the biochemical

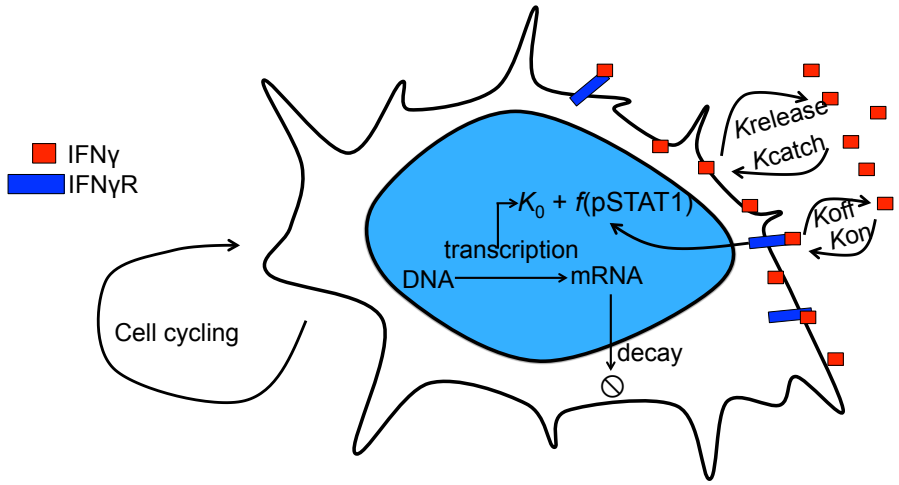

Figure 7.23: **Cartoon diagram of the mathematical model.** Once exogenous IFNγ is removed from the system, release of IFNγ from both the receptors and from the cell drive persistent signaling through the IFNγR until it is consumed below the threshold of signaling. Cells are allowed to proliferate and IFNγ leaves the system through endocytosis via the IFNγR.

interactions of IFNγ with the cell. A quantitative understanding of the IFNγ-cell interaction would enable us to eliminate some of the lipid candidates from figure Figure 7.22. Mass action kinetics were used to model binding of IFNγ to its receptor and to the cell (Figure 7.23). Once exogenous IFNγ is removed from the system, release of IFNγ from the cell drives persistent signaling through the IFNγ receptor until it is consumed to a quantity below the threshold of signaling.

Our updated mathematical model can be summarized using the following system of ordinary differential equations. It builds upon our previous model and incorporates cell proliferation because the timing of our experimental measurements is on the order of days: sufficient time for cells to undergo several rounds of division.

$$\begin{cases} \text{pSTAT1}([\text{IFN}\gamma]) \propto \frac{1}{1+\frac{\text{EC}_{50}}{[\text{IFN}\gamma]}}, \\ \frac{d[X-\gamma]}{dt} = k^X_{\text{catch}} \cdot [X] \cdot [\text{IFN}\gamma] - k^X_{\text{release}} \cdot [X-\gamma], \\ \frac{d[\text{IFN}\gamma]}{dt} = -k^X_{\text{catch}} \cdot [X] \cdot [\text{IFN}\gamma] + k^X_{\text{release}} \cdot [X-\gamma] - k_{cyc}\text{IFN}\gamma, \end{cases} \tag{7.1}$$

where X is the IFNγ non-signaling cell capture site, $X-\gamma$ is the IFNγ captured by X, k^X_{catch} and k^X_{release} are the kinetic catch and release rates of the $X-\gamma$ complex formation. For all of the parameter values used in the updated version of the model, refer to Table 3.1. Our evidence suggests that IFNγ is caught and released by the cell after it adheres to an as yet unknown molecule on the cell surface. To ease our parameterization efforts, we coarse-grained this interaction by modeling it as a single-step process. We stress that the catch and release rates encompass more than a single on and off rate, though because the exact mechanism of cell entry and exit is unknown, parameterizing a more biochemically exact model would be difficult and may not enhance our understanding of the system above that of a coarse-grained model. Importantly, we show below that our coarse-grained model is sufficient to account for all of our experimental observations.

To quantify the strength of IFNγ association with cells, we first determined the IFNγ cell association half-max (IFNγ_{50}). B16 IFNγR KO cells were exposed to different doses of fluorescent IFNγ for 7 hours, washed extensively and the cell-captured IFNγ was quantified by flow cytometry. The data were then fitted with a Hill function with a Hill coefficient of 1, and the IFNγ_{50} was computed from the fit (Figure 7.24). To ensure that cell association had reached equilibrium, we confirmed that the computed IFNγ_{50} was comparable between cells incubated with fluorescent IFNγ for 6 and 8 hours (not shown). From this experiment, we were able to assign a quantitative parameter that represents the strength of IFNγ

catch-and-release.

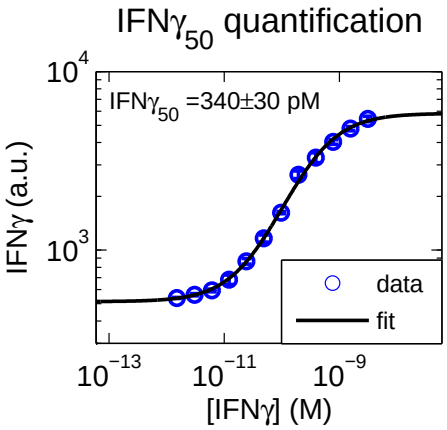

Figure 7.24: **Determining the IFNγ_{50} of IFNγ cell association.** B16 IFNγR KO cells were pulsed with the indicated doses of IFNγ-A647 for 7 hours, then washed extensively. Cell fluorescence was quantified by flow cytometry and the resulting data were fit with a Hill function with a coefficient of 1. The IFNγ_{50} was computed from the fit. Data plotted are the mean and s.e.m. (errorbars).

We used our model to predict the rate of IFNγ release from the cell. As a modeling target, we generated the pSTAT1 profile after removal of exogenous IFNγ from the system. Phosphorylated STAT1 is an ideal modeling target because it drives the downstream gene expression in our experiments. The pSTAT1 profile was generated using our experimentally determined EC_{50} of signaling (Figure 7.25a). and the concentration of free IFNγ generated by the model (Figure 7.25b).

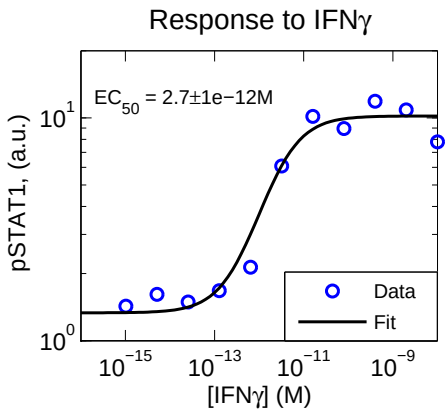

(a) **Determining the EC_{50} of IFNγ signaling.** B16 cells were stimulated with the indicated dose of IFNγ for 20 minutes. Cells were then fixed and permeabilized on ice, and stained for pSTAT1. Fluorescence was quantified by flow cytometry and the resulting data were fit with a hill function with a coefficient of 1.The EC_{50} was computed from the fit. Data is representative of at least 3 independent experiments.

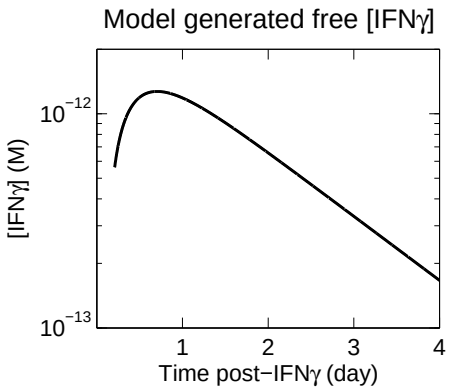

(b) **Model-generated concentration of free IFNγ.** The model generates a concentration of free IFNγ that decreases depending on the rate of endocytosis and cell proliferation. The pSTAT1 profile is generated from the free IFNγ concentration and the experimentally-determined EC_{50} of signaling.

Figure 7.25: Model parameters used to generate the pSTAT1 profile.

We kept IFNγ_{50} constant and varied the catch and release rates over several orders of magnitude (Figure 7.26). As a first approximation, we assumed that the number of IFNγ capture sites was on the same order of magnitude as the number of IFNγ receptors. We colored some of the plots orange and red because those pSTAT1 curves closely resembled the curve that we observed experimentally. The model predicted that IFNγ would have to be released from the cells on a timescale of several hours. This is somewhat unsurprising given that our evidence suggests IFNγ is internalized and released. We expect a process where IFNγ enters and exits the cell to be slower in comparison to canonical biochemical off rates.

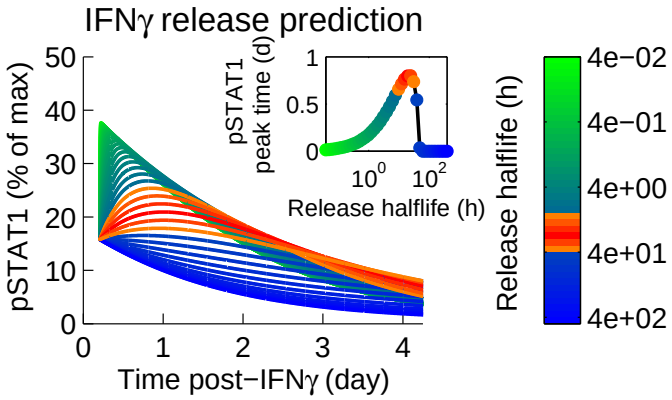

Figure 7.26: **Scanning the parameter space of IFNγ-cell catch and release rates.** The model was run by keeping the IFNγ_{50} constant, while varying the catch and release rates. The number of IFNγ binding sites on the cell was estimated to be on the same order of magnitude as the number of IFNγR (10^3). The pSTAT1 profile was generated based on the concentration of free IFNγ and the experimentally-measured EC_{50} of signaling.

We tested this prediction experimentally by performing a well-mixed competition experiment. B16 IFNγR KO cells were pulsed with fluorescent IFNγ, and then the media was replaced with an equimolar concentration of unlabeled IFNγ. The decay in cell fluorescence was quantified by flow cytometry and the resultant curve was fit with an exponential decay function (Figure 7.27). The halflife of IFNγ cell release from the cell is approximately 5h.

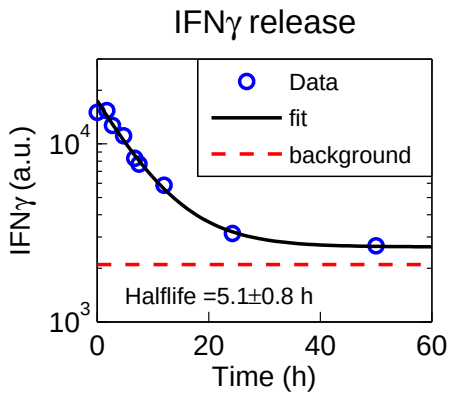

Figure 7.27: **Experimental measurement of the IFNγ-cell $k_{release}$.** B16 IFNγR KO cells were pulsed with 10nM IFNγ-A488 overnight while tumbling in a large volume of RPMI (in well-mixed conditions). The media was then replaced with 10nM unlabeled IFNγ and the decay in cell fluorescence was quantified by flow cytometry. The resultant data were fit with an exponential decay function and $k_{release}$ was computed from the fit. Data plotted is representative of 3 independent experiments.

We then substituted this release rate into our model, and used the IFNγ_{50} to infer theIFNγ cell capture rate (IFN$\gamma_{50} = \frac{k_{release}}{k_{catch}}$). We then fitted this model to the pSTAT1 data, keeping the number of cell binding sites as a free parameter (Figure 7.28a). Indeed, the number of association sites calculated per cell ($\approx 5 \times 10^3$) was on the same order of magnitude as the number of IFNγ receptors (2.5×10^3). Next, we used the pSTAT1 profile generated by the model to plot the mRNA dynamics and compared this to our data (Figure 7.28b). Using the experimentally derived IFNγ-cell association and dissociation rates, our model qualitatively describes the dynamics of pSTAT1 and mRNA.

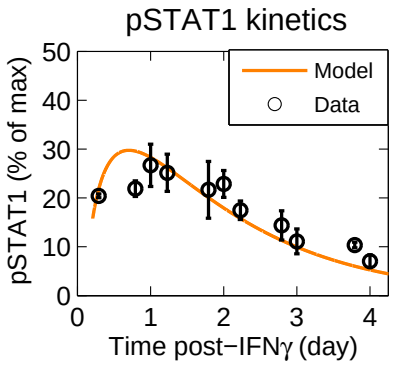

(a) **Fit of the model to the pSTAT1 data.** The experimentally-determined $IFN\gamma_{50}$ and $k_{release}$ were used to compute the k_{catch}. These values were then input into the model and the number of cell binding sites was kept as a free parameter. The model qualitatively describes the data given these parameters. Data plotted are the mean and s.e.m. (errorbars).

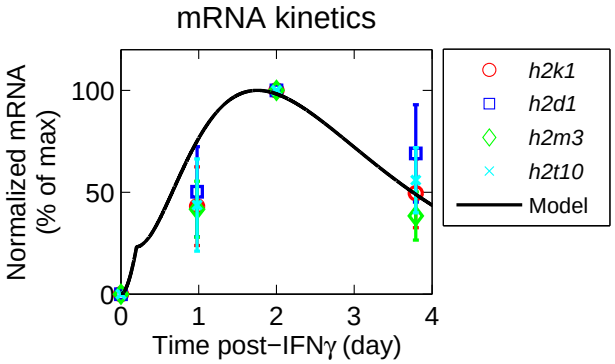

(b) **Fit of the model to the mRNA data.** The pSTAT1 data was used to compute the mRNA dynamics. Data plotted are the mean and s.e.m. (errorbars).

Figure 7.28: The model qualitatively recapitulates the experimental data.

7.5 Cell surface-exposed phosphatidylserine mediates IFNγ catch-and-release.

We reasoned that we could eliminate many of the lipid candidates based on their strength of IFNγ binding (Figure 7.22). Lipid-spotted membranes were probed with a thousand-fold lower IFNγ concentration (50pM). Indeed, incubating with a lower concentration of IFNγ constrained the lipids capable of binding to only three candidates: cardiolipin (CL), phosphatidylserine (PS), and phosphatidylinositol(4)phosphate (PI(4)P) (Figure **??**). The remaining lipids bind IFNγ with a much lower affinity so we did not focus on them as candidate molecules that mediate catch-and-release signaling.

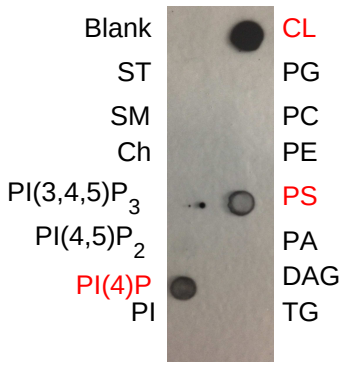

Figure 7.29: **A lower concentration of IFNγ constrains the lipid candidates based on their binding affinity.** Lipid-spotted strips were incubated with 50pM IFNγ, then washed and probed with a primary antibody directed against IFNγ. A secondary HRP-conjugated antibody directed against the primary isotype was then added and blots were developed and visualized. Code: CL: Cardiolipin; PG: Phosphatidylglycerol; PC: Phosphatidylcholine; PE: Phosphatidylethanolamine; PS: Phosphatidylserine; PA: Phosphatidic acid; DAG: Diacylglycerol; TG: Triglyceride; ST: Sulfatide; SM: Sphingomyelin; Ch: Cholesterol; PI(3,4,5)P_3: Phosphatidylinositol(3,4,5)Phosphate; PI(4,5)P_2: Phosphatidylinositol(4,5)Phosphate; PI(4)P: Phosphatidylinositol(4)Phosphate; PI: Phosphatidylinositol

In healthy cells, none of the three lipids are typically exposed on the cell surface. Cardiolipin is sequestered in mitochondrial membranes, while PS and PI(4)P are primarily localized to the plasma membrane inner leaflet [87]. We stained cells with lipid-specific reagents and used flow cytometry to detect the presence of these lipids on the plasma membrane outer leaflet. Specifically, PS was stained using fluorescently-labeled Annexin V, a protein that specifically binds PS in a $CaCl_2$-dependent manner. Cardiolipin and PI(4)P were stained with primary antibodies specific for each lipid and a fluorescently-tagged secondary antibody. As a negative control, a cohort of cells were stained with the secondary antibodies alone.

While CL and PI(4)P were undetectable, PS was present on the surface of live (Dapi-) B16 IFNγR KO cells (Figure 7.30). Notably, in fixed and permeabilized cells, both CL and PI(4)P were readily detectable, indicating that these antibodies are functional (Figure 7.31). Cardiolipin and PI(4)P were not cell surface-exposed,

so we eliminated them as candidates for IFNγ binding and focused on PS. PS typically decorates the plasma membrane inner leaflet, however when cells undergo apoptosis or necroptosis, PS flips onto the outer leaflet where it acts as an "eat me" signal for phagocytes by binding specific receptors present on their surface [21, 53]. Importantly, PS has been observed on the surface of live, viable tumor cells, and on T cells after T cell receptor-mediated activation [23, 76]. Thus, there are contexts where PS accumulates on the plasma membrane outer leaflet of live cells. Tumor expression of PS on the outer leaflet has been suggested to promote metastasis and may play a role in reducing cell immunogenicity by enhancing phagocytosis, thus promoting tumor immune-evasion [6, 48].

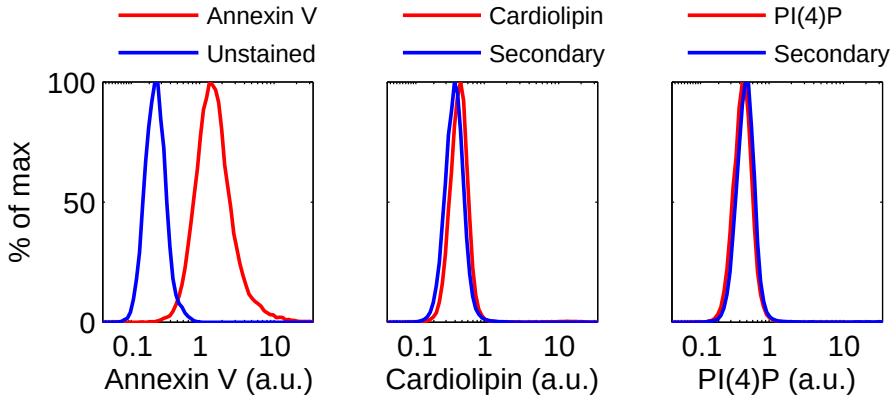

Figure 7.30: **Live, Dapi- cells express PS on the plasma membrane outer leaflet.** B16 IFNγR KO cells were stained with either: AnnexinV, αCardiolipin, or αPI(4)P. Dead cells were eliminated by gating cells of interest as Dapi-.

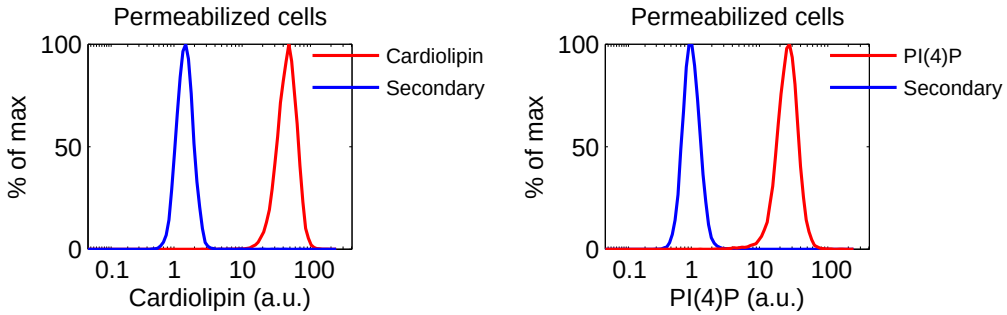

Figure 7.31: **Permeabilization of cells allows staining for intracellular lipids.** B16 IFNγR KO cells were fixed, permeabilized, and stained with either: αCardiolipin or αPI(4)P.

We imaged PS on the cell surface using Annexin V, and observed a punctate pattern similar to that of IFNγ (Figure 7.32a). This staining pattern was distinctly different than that of a dead cell, where Annexin V brightly stained the entire plasma membrane on rounded, detached cells (Figure 7.32b).

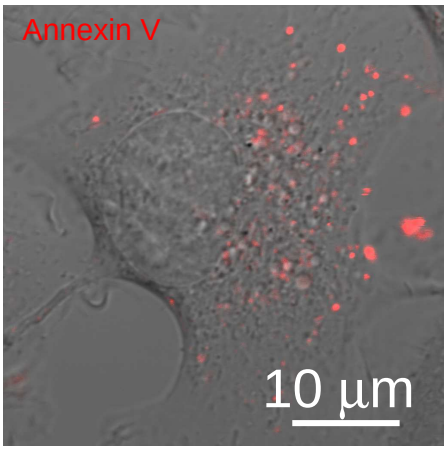

(a) **A. Annexin V assumes a punctate distribution on the surface of live cells.** B16 IFNγR KO cells were adhered to fibronectin-coated glass bottom culture dishes, then stained with fluorescently-labeled Annexin V, and imaged by confocal microscopy. Imaging is representative of at least 3 independent experiments.

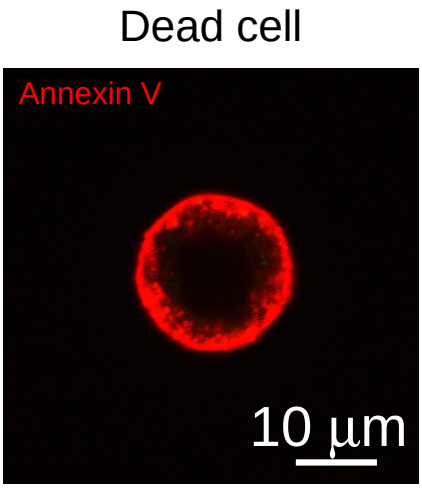

(b) **B. Annexin V brightly stains dead cells.**B16 IFNγR KO cells were adhered to fibronectin-coated glass bottom culture dishes, then stained with fluorescently-labeled Annexin V, and imaged by confocal microscopy. A rounded, detached cell was identified as dead.

Figure 7.32: The PS distribution differs markedly between live and dead cells.

Given that cholesterol co-localizes with IFNγ and its depletion reduces IFNγ cell capture (Figure 7.21), we hypothesized that if PS is the molecule responsible for binding, it would localize to cholesterol micro-domains. TF-cholesterol was introduced to cells and then imaged with Annexin V on live cells (Figure 7.33). Indeed Annexin V staining was observed in cholesterol-containing lipid micro-domains.

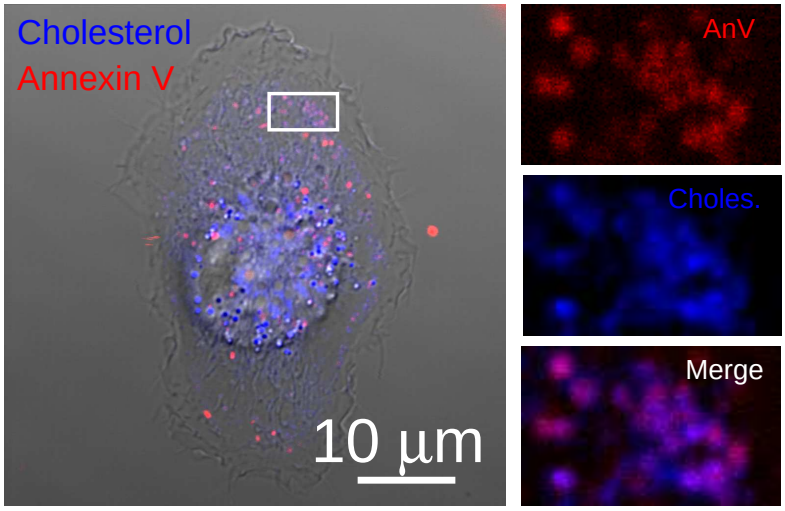

Figure 7.33: **PS is co-localized with cholesterol.** First, TF-cholesterol was introduced into B16 IFNγR KO cells. TF-MβCD complexes were mixed in PBS with PBS-washed cells for 5 minutes at 37°C. Cells were then washed in RPMI and adhered to fibronectin-coated glass-bottom culture plates. Cells were then stained with fluorescently-labeled Annexin V and imaged by confocal microscopy.

To show that PS is necessary for IFNγ binding, we tested whether treatment with Annexin V is capable of blocking IFNγ-binding to PS. Cells were treated with 50nM Annexin V, and then an IFNγ-capture assay was performed (Figure 7.11). This dose of Annexin V strongly reduced IFNγ cell capture relative to cells treated with the $CaCl_2$ buffer control (Figure 7.34).

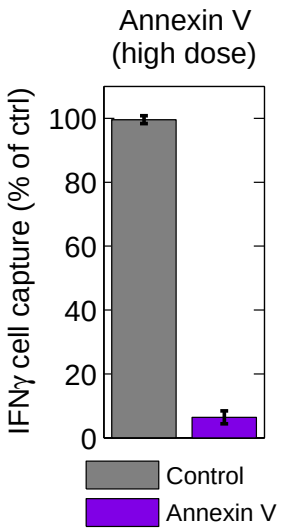

Figure 7.34: **High-dose Annexin V blocks IFNγ cell capture.** B16 IFNγR KO cells were first treated with a high-dose of Annexin V. Specifically, cells were treated with 50nM Annexin V for 15min at 37°C. After, cells were kept in Annexin V, and 50pM IFNγ diluted in Annexin V-binding buffer supplemented with 3% fetal calf serum (FCS). Data plotted are mean and s.e.m. (errorbars) and representative of at least 3 independent experiments.

In our experimental settings, it's unclear what mechanism controls the spatial distribution of phosphatidylserine and cholesterol on the plasma membrane. The ATP-binding cassette transporter-1 (ABCA-1) plays a role in both cholesterol and PS lipid bilayer distribution [28, 88]. Therefore one could speculate that the membrane localization of ABCA-1 explains the co-localization of both cholesterol and PS. However, one mystery that remains is why the depletion of cholesterol both transiently, permanently, and at the level of biosynthesis alters IFNγ cell capture. This result suggests that cholesterol depletion inhibits internalization of IFNγ. Given the importance of cholesterol for caveolae-mediated endocytosis, we predict that the importance of cholesterol lies in its ability to serve as a scaffold for caveolin proteins [57].

The observation that both IFNγ and PS were localized to cholesterol micro-

domains strongly suggested that they would also co-localized with one another. We sought to image IFNγ and Annexin V together. To circumvent blocking of IFNγ by Annexin V, we stained cells with a 50-fold lower dose of Annexin V. Indeed, IFNγ and Annexin V were nearly super-imposable (Figure 7.35). These data reveal that PS directly binds IFNγ and is necessary for cell capture of IFNγ.

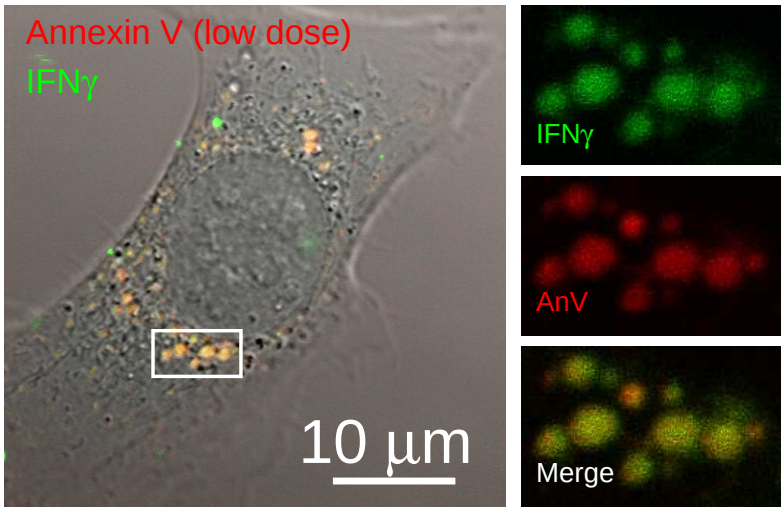

Figure 7.35: **Low-dose Annexin V permits dual imaging of PS and IFNγ.** B16 IFNγR KO cells were first adhered to fibronectin-treated glass-bottom culture dishes. Next, cells were treated with a low-dose of Annexin V. Specifically, cells were treated with a dose of Annexin V titrated down 10-fold from the manufacturer protocol for 15min at 37°C. Finally, cells were incubated with IFNγ-A647 for several hours. Cells were then washed and imaged by confocal microscopy. Imaging is representative of 2 independent experiments.

We reasoned that the quantity of IFNγ captured by cells would scale positively with the amount of PS on the cell outer leaflet. To test this, we created three classes of cells: Live, dying, and dead. Dying cells were made via heat shock, and cells were killed using staurosporine. These cells were mixed and gated into Dapi low, medium, and high populations (Figure 7.36). The cells were then stained with either Dapi and Annexin V, or Dapi and IFNγ-A647. Indeed, populations with greater PS staining also exhibited increased IFNγ cell association.

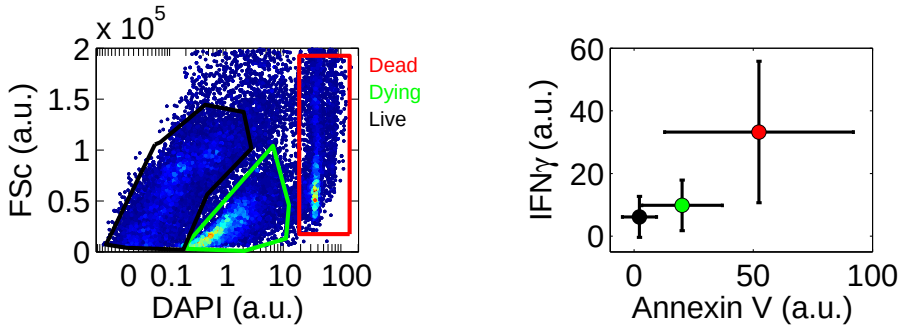

Figure 7.36: **Dead and dying cells bind increased IFNγ.** B16 IFNγR KO cells were split into 3 fractions, live, dying, and dead cells. After trypsinizing and washing cells from culture, approximately 95% are live, as assessed by Dapi exclusion. Dying cells were generated by heat shocking live cells for 30s in a water bath set at 42°C. Dead cells were generated by treating live cells with 5μM staurosporine for 2 hours at 37°C. The 3 cell fractions were mixed and immediately split into 2 staining groups. One group was stained with Dapi and the manufacturer suggested concentration of Annexin V. The other group was stained with Dapi and IFNγ-A647. Fluorescence was determined by flow cytometry. Cells were gated based on their level of Dapi incorporation as live (Dapi^{lo}), dying (Dapi^{med}), and dead (Dapi^{hi}). The graph on the right shows the population geometric mean fluorescence for each gate, and the population spread (errorbars).

Given that IFNγ binds to PS, we decided to check whether the panel of cell lines tested earlier also present PS on their plasma membrane outer leaflet. We stained CH12, Hek293T, RAW, H460, and Mel2 with fluorescently-labeled Annexin V and Dapi. In all cell lines, Dapi^{hi} cells stained very brightly with Annexin V (data not shown). However, when we gated on live cells (Dapi^{lo}), we observed that all of the cell lines presented PS on their outer membrane (Figure 7.37). This observation is consistent with results from our earlier experiments (Figure 7.8b).

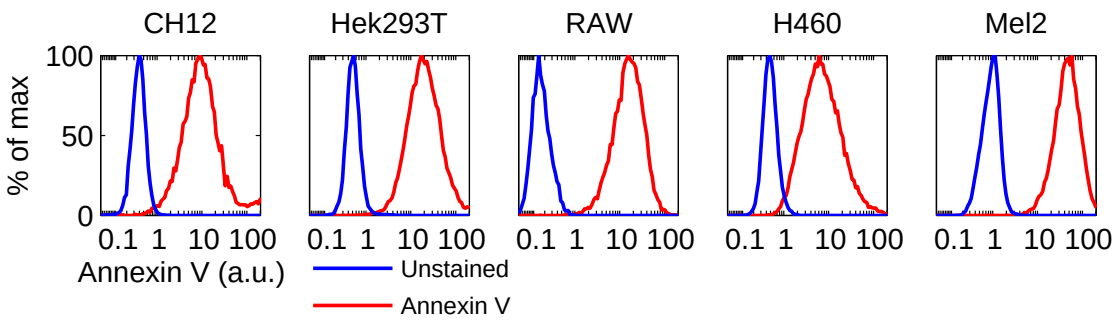

Figure 7.37: **Live cells of diverse origin present PS on the plasma membrane outer membrane.** All of the indicated cell lines were stained with Annexin V-A488 according to manufacturer instructions.

CHAPTER 8

FUNCTIONAL CONSEQUENCES FOR CATCH-AND-RELEASE COMMUNICATION

8.1 Catch-and-release communication could enable communication between spatio-temporally separate cells.

In a lymphoid or tumor environment, T cells produce IFNγ for only a short period of time before disengaging and migrating elsewhere [32, 34, 35]. However, if IFNγ is caught by cells in the vicinity where it was produced, its strikingly slow release time could permit signaling to different cell types, which migrate into the environment later (Figure 8.1). Thus cells that are separated by both space and time could communicate using cytokine catch-and-release. Macrophages typically recognize PS via specific receptors, enabling phagocytosis of the PS+ cell [21, 53]. Catch-and-release signaling may be a mechanism by which T cells deposit cytokines on PS+ cells in order to communicate with phagocytes that encounter the cell later. We sought to test whether the IFNγ bound to PS on tumor cells was sufficient to activate macrophages.

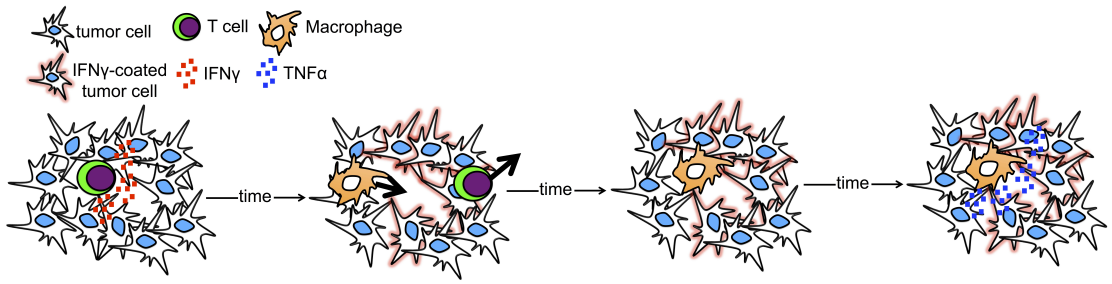

Figure 8.1: **Catch-and-release signaling could enable communication between spatio-temporally separate cells.** In a tumor environment, activated T cells produce IFNγ for only about 5 hours before dissociating and migrating elsewhere. However, if IFNγ is sequestered by surrounding tumor cells, its lifetime in the environment is dramatically lengthened. This would allow it to continue signaling to tumor cells, and potentially to another cell type that migrated into the environment later. For instance, if a macrophage migrated to the area later, it may be able to respond to residual IFNγ, become activated and possibly produce new cytokines like tumor necrosis factorα (TNFα). Hence the T cell and the macrophage were never in the same place at the same time, but they are still able to communicate.

To this end, we further developed our original IFNγ sensor cell assay. As IFNγ-pulsed cells, we used B16 IFNγR KO melanoma cells. As sensors, we used either BALB/c wild type (WT), or IFNγR KO murine bone marrow-derived macrophages (BMDM). We chose B16 IFNγR KO cells as cytokine-sharing cells to avoid potentially confounding effects due to production of inflammatory cytokines by WT B16 cells in response to IFNγ. To generate BMDM, bone marrow was harvested from the hind femurs and tibia of BALB/c WT or IFNγR KO mice. Bone marrow was washed, and differentiated for 7 days in teflon bags in the presence of 10ng/mL mouse M-CSF. Media and cytokines were refreshed every 2 days. After 7 days, approximately 50% of the bone marrow derived cells were CD11b+ (not shown).

Melanoma cells were pulsed with 10nM IFNγ for 5h, then washed and co-cultured with either WT or IFNγR KO BMDM. We quantified the response to IFNγ by expression of inducible Nitric Oxide Synthase (iNOS), a canonical

macrophage response to the cytokine (Figure 8.2a). Macrophage expression of iNOS enables their production of reactive nitrogen species, which facilitate killing of engulfed, intracellular pathogens.

IFNγ-pulsed melanoma cells up-regulated macrophage expression of iNOS in WT but not IFNγR KO BMDM (Figure 8.2b). Therefore, PS-bound IFNγ is sufficient to activate macrophages.

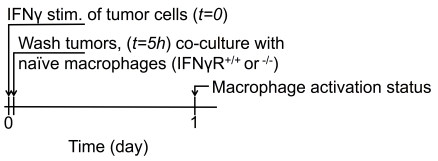

(a) **Melanoma-Macrophage co-culture experimental diagram.** B16 IFNγR KO cells were pulsed with 10nM IFNγ or mock-pulsed for 5h, then washed extensively. Pulsed or un-pulsed cells were then co-cultured with day 7, WT or IFNγR KO BMDM for 1 day.

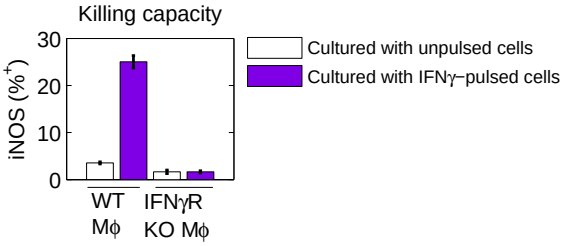

(b) **IFNγ shared by melanoma cells is sufficient to activate macrophages.** After 1 day of co-culture, cells were harvested using ice cold 5mM EDTA in PBS and gentle agitation. Cells were fixed, permeabilized, and then stained for CD11b and iNOS. Fluorescence was quantified by flow cytometry. Data plotted is the mean and s.e.m. (error bars) and representative of at least 3 independent experiments.

Figure 8.2: IFNγ shared by melanoma cells is sufficient to activate macrophages.

Next, dual administration of IFNγ and tumor necrosis factorα (TNFα) are known to cooperatively induce cell death [8, 50]. Therefore, we asked if cytokine catch-and-release could enhance cell death in response to sequential treatment with these cytokines. B16 WT cells were pulsed with IFNγ, and then washed. After washing, one cohort of cells was left untreated, one was incubated with TNFα, and the final cohort was incubated with TNFα and neutralizing antibodies directed against IFNγ (Figure 8.3a). After 24 hours, cell death was quantified by

Dapi incorporation. Indeed, in conditions where catch-and-release signaling was permitted, TNFα boosted cell death (Figure 8.3b). This experiment illustrates an additional functional consequence for catch-and-release signaling: staggered response to IFNγ and TNFα can enhance cytotoxicity due to the slow release of IFNγ.

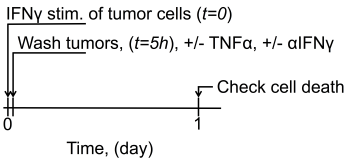

(a) **A. Staggered IFNγ TNFα treatment experimental diagram.** B16 WT cells were pulsed with 10nM IFNγ or mock-pulsed for 7h, then washed extensively. After washing, one cohort of IFNγ pulsed cells were cultured with only 10nM TNFα or 10nM TNFα and neutralizing antibodies directed against IFNγ. Cell death was quantified after 1 day of culture.

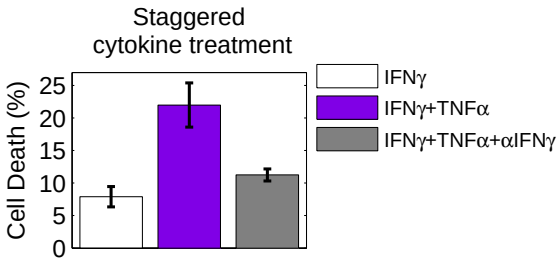

(b) **B. Catch-and-release signaling boosts subsequent TNFα-mediated killing.** After 1 day of culture, B16 viability was quantified by incorporation of Dapi. Data plotted is the mean and s.e.m. (errorbars) and representative of 2 independent experiments.

Figure 8.3: Catch-and-release signaling boosts subsequent TNFα-mediated killing.

CHAPTER 9

TESTING WHETHER CYTOKINE CATCH-AND-RELEASE IS APPLICABLE TO OTHER CYTOKINES

Finally, we sought to determine whether other cytokines can also bind to PS. To this end, we performed a lipid blot experiment using 5nM of the following cytokines: Interleukin-2 (IL2), Interleukin-4 (IL4), Interleukin-6 (IL6), Interleukin-10 (IL10), Interleukin-12 (IL12), Interleukin 23 (IL23), Interleukin 17 (IL17) and TNFα. We chose this concentration of cytokine because it is a dose that may reasonably accumulate depending on conditions in vivo. We observed that none of these cytokines bound to any of the lipids spotted onto the strips, with the exception of IL12 and IL23 (and data not shown), (Figure 9.1, Figure 9.2). We observed binding to a similar collection of lipids as IFNγ: cardiolipin, sulfatide, phosphatidylserine, and phosphatidylinositol(4)phosphate. Importantly, both IL12 and IL23 obviously interacted most strongly with PS.

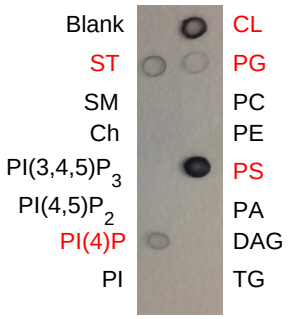

Figure 9.1: **IL23 binds to a variety of anionic phospholipids.** A lipid spotted strip was blocked, then exposed to 5nM IL23 overnight at 4°C. Next, blot were washed then probed with a primary antibody directed against IL23, a secondary antibody directed against Rat, and developed using HRP substrate. Blot was exposed for 5 minutes before developing. Blot is representative of 2 independent experiments. Code: CL: Cardiolipin; PG: Phosphatidylglycerol; PC: Phosphatidylcholine; PE: Phosphatidylethanolamine; PS: Phosphatidylserine; PA: Phosphatidic acid; DAG: Diacylglycerol; TG: Triglyceride; ST: Sulfatide; SM: Sphingomyelin; Ch: Cholesterol; $PI(3,4,5)P_3$: Phosphatidylinositol(3,4,5)Phosphate; $PI(4,5)P_2$: Phosphatidylinositol(4,5)Phosphate; PI(4)P: Phosphatidylinositol(4)Phosphate; PI: Phosphatidylinositol

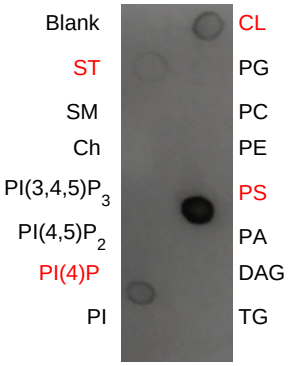

Figure 9.2: **IL12 binds binds to a variety of anionic phospholipids.** A lipid spotted strip was blocked, then exposed to 5nM IL12 overnight at 4°C. Next, blot were washed then probed with a primary antibody directed against IL12, a secondary antibody directed against Rat, and developed using HRP substrate. Blot was exposed for 5 minutes before developing. Blot is representative of 2 independent experiments. Code: CL: Cardiolipin; PG: Phosphatidylglycerol; PC: Phosphatidylcholine; PE: Phosphatidylethanolamine; PS: Phosphatidylserine; PA: Phosphatidic acid; DAG: Diacylglycerol; TG: Triglyceride; ST: Sulfatide; SM: Sphingomyelin; Ch: Cholesterol; $PI(3,4,5)P_3$: Phosphatidylinositol(3,4,5)Phosphate; $PI(4,5)P_2$: Phosphatidylinositol(4,5)Phosphate; PI(4)P: Phosphatidylinositol(4)Phosphate; PI: Phosphatidylinositol

These data suggest that catch-and-release signaling is likely not distinctive of IFNγ, but may be applicable to other cytokines, chemokines, and growth factors. We next tested whether, similar to IFNγ, IL12 could also bind to cells in a PS-dependent manner. To this end, we repeated the cytokine capture assay using IL12 (Figure 7.11). B16 IFNγR KO cells were treated with 50nM Annexin V, and then an IL12-capture assay was performed with IL12 added at 50pM. This dose of Annexin V strongly reduced IL12 cell capture relative to cells treated with the $CaCl_2$ buffer control (Figure 9.3).

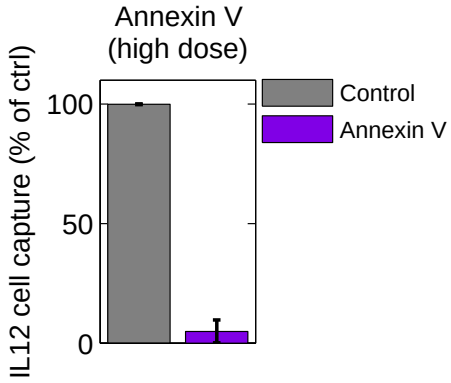

Figure 9.3: **IL12 also binds to cells in a PS-dependent manner.** B16 IFNγR KO cells were first treated with a high-dose of Annexin V. Specifically, cells were treated with 50nM Annexin V for 15min at 37°C. After, cells were kept in Annexin V, and 50pM IL12 was diluted in Annexin V-binding buffer supplemented with 3% fetal calf serum (FCS). Depletion of IL12 from the media was quantified by bead-based ELISA. Data plotted are the mean and s.e.m. (errorbars) and representative of 3 independent experiments.

Finally, we tested whether IL12 can participate in catch-and-release communication. Since IL12 can potentiate IFNγ release by macrophages, we assayed whether IL12 shared from B16 cells results in macrophage secretion of IFNγ. B16 IFNγR KO cells were pulsed with 10nM IL12 for 5h, then washed. B16 cells were then co-cultured with BMDM for 1 day. Supernatant was harvested after 1 day of co-culture and assayed for accumulation of IFNγ. Indeed, when macrophages were co-cultured with IL12-pulsed B16 cells, they released IFNγ, indicating that

IL12 can also participate in cytokine catch-and-release (Figure 9.4).

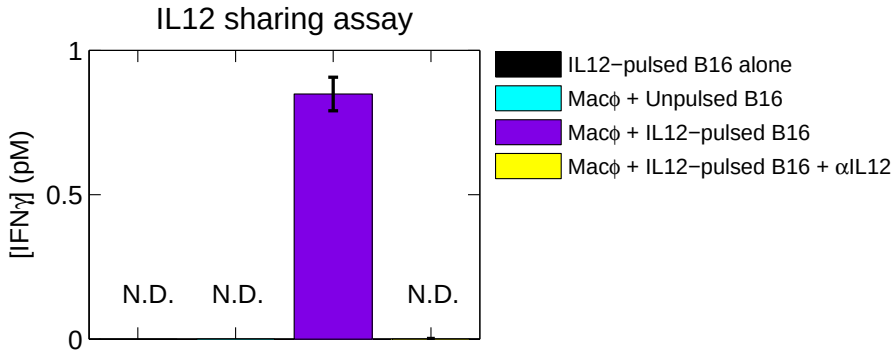

Figure 9.4: **IL12 participates in cytokine catch-and-release.** B16 IFNγR KO cells were pulsed with 10nM IL12 for 5h, then washed. B16 cells were then co-cultured with BMDM for 1 day. Supernatant was harvested after 1 day of co-culture and assayed for accumulation of IFNγ by bead-based ELISA. Where indicated, αIL12 was added to the culture. N.D. stands for "not detected." Data plotted are the mean and s.e.m. (errorbars) and representative of 3 independent experiments.

CHAPTER 10

SUMMARY

We discovered a novel mechanism of cell-to-cell communication, which we named cytokine catch-and-release communication. In this mode of signaling, IFNγ binds to PS exposed on the plasma membrane outer leaflet, is internalized, and is then slowly released back to the microenvironment. The halflife of cytokine release from cells is on the order of 5 hours. Once released, the cytokine signals to nearby cells in a proximity-dependent manner. This mechanism enables transiently produced cytokines to signal over a timescale much longer than that of their secretion. The pro-inflammatory cytokine IFNγ is secreted by activated T cells for 5.9$\pm$3.6h [32]. However, catch-and-release communication enabled IFNγ to act over a timescale of 2-3 days, after cells were initially exposed for only a few brief hours.

Catch-and-release communication enabled melanoma cells to continue up-regulating genes in the antigen presentation pathway for several days after their initial exposure to IFNγ. Long-term up-regulation of the antigen presentation pathway had important downstream consequences for T cell activation. Specifically, by lengthening the period of enhanced antigen presentation, melanoma cells were susceptible to T cells for a greater duration of time. In addition, sharing of IFNγ from melanoma cells was sufficient to activate naive macrophages to up-regulate expression of genes that promote production of reactive nitrogen species. This experiment suggested that two cells (a cytokine producer cell and a different, cytokine consumer cell) separated by both space and time may be able to communicate. Finally, this mechanism enabled enhanced TNFα-mediated killing of IFNγ-pulsed cells by extending the time period that cells responded to IFNγ.

Catch-and-release signaling is not unique to mouse or melanoma cells, but is instead a general feature of diverse cell types including human cells, and cell lines derived from both primary and tumor cells. Exposure of PS on the plasma membrane outer leaflet was once thought to be characteristic of dead or dying cells. However, it is increasingly clear that there are many contexts where PS is exposed on the outer leaflet in both healthy and cancerous, viable cells [76, 86, 23]. Importantly, the surface distribution of PS on live cells is much different than that of dead cells. On live cells, PS appears to occupy cholesterol-rich lipid microdomains and assumes a punctate pattern of staining. In contrast, dead cells exhibit uniform, bright staining over the entire plasma membrane, indicating the flip of PS from the inner to outer leaflet [21]. Furthermore, we observed that the cytokines IL12 and IL23 also binds to both purified PS and to cells in a PS-dependent manner, suggesting that catch-and-release signaling is likely not distinctive to IFNγ, but may be applicable to other cytokines, chemokines, and growth factors.

CHAPTER 11

DISCUSSION

11.1 Using dynamics, modeling, and perturbation-style biology to uncover novel mechanisms of gene regulation.

Three specific strategies served as the thrust for our study. First, we tracked the dynamics of the cell response to an extracellular stimulus at many levels ranging from transcription factor activation (pSTAT1), to RNA, to protein. This allowed us to unify our understanding of the IFNγ response at the level of signaling with downstream functional consequences, such as protein expression. Second, we used targeted, perturbation-style experiments to test specific hypotheses, parameterize our mathematical model, and ultimately uncover the mechanism by which catch-and-release signaling operates.

Of late, tracking the dynamics of RNA or protein on a systems-wide scale has been an attractive strategy to understand what mechanisms control gene regulation [67, 68, 38]. While this strategy can certainly be informative and has yielded insights into transcriptional and translational regulation, there are limitations to what one can infer from what is essentially a single dataset. In addition, when these studies employ mathematical modeling, it is difficult, if not impossible to appropriately parameterize the model without making un-tested assumptions that may or may not be true. Oftentimes these datasets are effective at generating hypotheses, but fall short in following through and rigorously testing those hypotheses. Definitive conclusions and a more sophisticated understanding of the system are gleaned when projects synthesize systems-scale experiments and experiments designed to

test specific hypotheses [61, 77, 12].

Third, we used a mathematical model to both test our mechanistic understanding of the system and guide subsequent experiments. As datasets continue to grow in richness and size, mathematical modeling will also become increasingly necessary to distill key features.

11.2 Implications for cytokine catch-and-release communication in the immune system.

In vivo, an appropriate immune response relies on temporally coordinated waves of immune cell migration, activation, and cytokine secretion [52, 11, 19, 41, 40]. Lymphocyte differentiation depends primarily on exposure to specific cytokine cocktails induced in response to a given pathogen [91]. "First responder" cells present at the site of injury or infection generate the first wave of cytokines [9, 4]. Given the transient nature of cytokine production, what mechanisms ensure that subsequent waves of infiltrating immune cells migrate rapidly enough to access first-wave cytokines? This question can be answered in part by chemokines, which guide circulating immune cells to the site of infection in a timely manner [11, 47, 63, 40]. However, cells exhibit variable migratory responses to chemokines, resulting heterogeneity in the timing of cell arrival. Perhaps catch-and-release signaling provides a temporal buffer for infiltrating immune cells by extending the duration over which cytokines persist in the environment. This may be particularly relevant to T helper-type I differentiation, which relies on sequential positive feedback loops between IFNγ and IL12 [74].

Indeed, this type of temporally buffered signal has been observed in other systems. For example, migrating neutrophils leave chemokine-enriched trails in their wake [47]. These trails were composed of membranous bits of neutrophil uropods, which were subsequently scavenged by following T cells. The authors speculated that this mechanism enabled the chemokine to persist in the environment longer than it would as a soluble molecule.

11.3 Implications of cytokine catch-and-release communication for other systems.

Macrophages are polarized towards an inflammatory phenotype by exposure to pro-inflammatory cytokines, namely IFNγ [56]. Inflammatory macrophages can be characterized based on their production of cytokines like TNFα and IL6, chemokines like CCL2, high expression of MHC class II, and expression of enzymes that generate reactive nitrogen species like iNOS. Inflammatory macrophages are critical for eradication of pathogens and, in some cases can improve immune-mediated rejection of tumors. On the other hand, these macrophages can contribute to the pathophysiology of myriad inflammatory diseases including atherosclerosis, cancer, and insulin resistance [54].

Atherosclerosis is a driver of heart attack and stroke. An inflammatory circuit between macrophages and pro-inflammatory cytokines is a key driver of atherosclerosis. In fact, disrupting inflammatory signaling and ablating macrophages often ameliorates the disease phenotype by slowing the progression of atherosclerotic plaques. In addition, outer leaflet presentation of PS and defective clearance of apoptotic/necrotic cells is a hallmark of advanced atherosclerotic plaques. It is

tempting to speculate that accumulation of IFNγ on PS in the necrotic core of the plaque could lay an inflammatory foundation that drives macrophage polarization and exacerbates disease. Furthermore, identification of the peptide moiety of IFNγ and IL12 that binds PS could enable specific targeting of PS in areas where the phospholipid is presented at high levels on the plasma membrane outer leaflet, such as atherosclerotic plaques and tumors. This may be an effective strategy for drug delivery.

11.4 Structural considerations of cytokine-PS interactions.

What biophysical characteristics enable binding of IFNγ, IL12, and IL23 to PS and can we speculate about this biochemistry to explore other possible protein-lipid interactions? Our experiments revealed that all three cytokines bind to phospholipids with negatively charged head groups, such as PS, cardiolipin, and phosphatidylinositol(4)phosphate. This suggests that a positively charged, polybasic region of the cytokine mediates binding. Examination of IFNγ structure revealed a sequence of exposed, cationic domains rich in arginine and lysine residues in the carboxy terminus [72]. Indeed, this region of IFNγ has proven essential for electrostatic interaction with negatively charged regions of the glycosaminoglycan heparan sulfate. IL12 and IL23 also contains a sequence of basic amino acids near the carboxy terminus of the p40 subunit [89]. Similarly, the bacterial endolysin PlyC binds strongly to PS via a cationic region of the protein rich in arginines and lysines [79]. In this study the authors discovered that PlyC first binds PS via cationic residues and is then internalized. While they were unable to decipher the specific mechanism of internalization, they did determine that internalization is cholesterol-dependent. We also observed an important role for cholesterol in

mediating association of IFNγ with cells.

The study of protein-lipid interactions has been relatively limited compared to protein-protein interactions, due largely to technical challenges and a dearth of experimental tools. The importance of developing new tools to characterize protein-lipid interactions is underscored by increasing evidence describing how these interactions modify protein function. From a clinical perspective, an understanding of the key amino acid residues and structural conformation necessary for protein-PS binding could enable the rational design of PS-targeting peptides. This may be valuable given the recent interest in developing monoclonal antibodies designed to target tumor cell plasma membrane-expressed PS [69, 26]. On the other hand, this information could enable prevention of off target effects where a peptide-based drug is unintentionally sequestered by PS presenting cells.

Sequestration of IFNγ by PS+ cells may be beneficial in some contexts, but deleterious in others. For example, IFNγ production by activated immune cells in tumors is often seen as a positive prognostic factor, yet the infusion of recombinant IFNγ in cancer clinical trials has largely failed [90, 49]. Administration of recombinant IFNγ often leads to significant, debilitating toxicity in the patient. Perhaps excessively large concentrations of IFNγ accumulate in PS+ tissues, leading to toxicity. Our discovery that IFNγ binds PS may provide an opportunity for fresh interpretation of some of the paradoxical results that emerged from the IFNγ clinical trials.

CHAPTER 12

FUTURE WORK

12.1 Identify the peptide moiety of IFNγ, IL12, and IL23 responsible for PS binding.

Identification of the specific residues of IFNγ, IL12, and IL23 responsible for PS binding is an important goal with potentially translational implications. PS is a phospholipid with a negatively charged head group [87]. Previously, binding of the bacterial endolysin PlyC to the negatively charged PS head was shown to depend on a sequence of positively charged amino acids [79]. IFNγ has a polybasic sequence rich in arginine and lysine that is known to mediate electrostatic interaction between the cytokine and negatively charged moieties of the glycosaminoglycan heparan sulfate [72]. In addition, IL12 and IL23 also has a arginine/lysine rich region near the c-terminus of the p40 subunit [89].

In future work, we will identify the region of IFNγ, IL12, and IL23 necessary for binding to PS. We will establish a screen using liposomes constructed from a mixture of phosphatidylcholine and phosphatidylserine. Our lipid blots established that None of the cytokines bound to phosphatidylcholine. In addition, we will generate fluorescently-tagged truncations of the IFNγ, IL12, and IL23 proteins. PS/PC liposomes will be pulsed with dose titrations of fluorescent peptides, then binding will be quantified by flow cytometry. Once we have identified the peptides capable of high-affinity binding to PS, we will check their specificity by assessing PS-specific binding to actual cells.

12.2 Characterize the mechanism of cytokine internalization

We observed that some IFNγ is present on the cell surface or just under the cell surface, but susceptible to release mediated by low pH treatment. Another fraction of IFNγ is inside the cytoplasm and resistant to low pH. This indicates that PS mediates some type of IFNγ internalization. We were unable to block cell capture of IFNγ by pre-incubating cells with an inhibitor of clathrin and dynamin-dependent endocytosis, indicating PS-IFNγ internalization is independent of this pathway.

In other work, PS mediated uptake of the bacterial endolysin PlyC via cholesterol-rich lipid rafts [79]. The fact that cholesterol and lipid rafts are required for uptake in both our work and in other work suggests a role for caveolae-dependent endocytosis, which is clathrin-independent [44]. Consistent with some of our results, Shen et al., were able to rule out other modes of internalization including macropinocytosis and clathrin-dependent endocytosis using drugs that inhibit each pathway. On the other hand, it is possible that IFNγ is internalized via flipping of PS from the outer to inner leaflet via a flippase enzyme. Annexin A5, which binds PS, nanomecanically elicits membrane invagination and formation of small vesicles that pinch off inside the cell in a form of internalization similar to, but distinct from macropinocytosis [42].

Taken together, these data suggest that PS-IFNγ internalization occurs via either caveolae-dependent endocytosis, action of a phospholipid flippase, or non-canonical pinocytosis similar to that observed for Annexin V. Our result that filipin inhibits IFNγ catching argues for a role of caveolae because it chelates cholesterol,

an important component of caveolae-rich microdomains. We will test for the role of caveolae-dependent internalization by also inhibiting tyrosine kinases involved in the pathway. Cells will be pre-treated with genistein, an inhibitor of the protein tyrosine kinases necessary for caveolae-dependent endocytosis, then we will perform the IFNγ capture assay. We will also stain for Cav1 and observe whether IFNγ co-localizes with caveolae in lipid microdomains. Finally, we will conjugate gold nanoparticles to IFNγ and perform transmission electron microscopy to image intracellular movement of IFNγ with greater resolution than that afforded by fluorescence microscopy.

12.3 Explore catch-and-release signaling in vivo.

What role does catch-and-release signaling play in vivo? This mechanism of signaling lengthens the temporal duration of the cytokine in the microenvironment. We have initiated a collaboration with the lab of Dr. Raza Zaidi at Temple University to investigate this in the context of the tumor microenvironment. The Zaidi lab has evidence that exposure of some tumor cell types to IFNγ actually promotes lung metastasis (unpublished data). Given the important role of IFNγ in promoting antigen presentation on tumor cells and enhancing T cell recognition, it's possible that the pro-metastatic effects of IFNγ extend to the microenvironment of the tumor, rather than to tumor cells themselves. We will conduct pilot experiments using an intravenous (I.V.) injected melanoma cell line B2905. This cell line provides an excellent model system because, in contrast to the B16 melanoma line, it harbors mutations associated with human disease. Our collaborators are generating a clean IFNγR KO B2905 cell line using the CRISPR/Cas9 system.

We plan to use these cells to examine the effect of IFNγ shared from cells as opposed to the effect of IFNγ acting on cells. B2905 WT or IFNγR KO cells will be pulsed with IFNγ and washed, or pulsed with IFNγ, washed, and acid stripped to remove cell-associated IFNγ. Then cells will be injected I.V. into mice. Tumors will be allowed to grow, then lung metastases will be assessed. This system will allow us to distinguish between the effect that IFNγ may have on promoting metastasis by acting on tumor cells themselves, versus its potential effect due to cell-sharing with other cells in the microenvironment.

CHAPTER 13

BIBLIOGRAPHY

[1] D. S. Aaronson and C. M. Horvath. A road map for those who don't know jak-stat. *Science*, 296(5573):1653–5, 2002.

[2] S. Agarwal and A. Rao. Modulation of chromatin structure regulates cytokine gene expression during t cell differentiation. *Immunity*, 9(6):765–75, 1998.

[3] F. Altare, A. Durandy, D. Lammas, J. F. Emile, S. Lamhamedi, F. Le Deist, P. Drysdale, E. Jouanguy, R. Doffinger, F. Bernaudin, O. Jeppsson, J. A. Gollob, E. Meinl, A. W. Segal, A. Fischer, D. Kumararatne, and J. L. Casanova. Impairment of mycobacterial immunity in human interleukin-12 receptor deficiency. *Science*, 280(5368):1432–5, 1998.

[4] S. Ariotti, M. A. Hogenbirk, F. E. Dijkgraaf, L. L. Visser, M. E. Hoekstra, J. Y. Song, H. Jacobs, J. B. Haanen, and T. N. Schumacher. T cell memory. skin-resident memory cd8(+) t cells trigger a state of tissue-wide pathogen alert. *Science*, 346(6205):101–5, 2014.

[5] M. Ashburner, C. A. Ball, J. A. Blake, D. Botstein, H. Butler, J. M. Cherry, A. P. Davis, K. Dolinski, S. S. Dwight, J. T. Eppig, M. A. Harris, D. P. Hill, L. Issel-Tarver, A. Kasarskis, S. Lewis, J. C. Matese, J. E. Richardson, M. Ringwald, G. M. Rubin, and G. Sherlock. Gene ontology: tool for the unification of biology. the gene ontology consortium. *Nat Genet*, 25(1):25–9, 2000.

[6] A. Bondanza, V. S. Zimmermann, P. Rovere-Querini, J. Turnay, I. E. Dumitriu, C. M. Stach, R. E. Voll, U. S. Gaipl, W. Bertling, E. Poschl, J. R. Kalden, A. A. Manfredi, and M. Herrmann. Inhibition of phosphatidylser-

ine recognition heightens the immunogenicity of irradiated lymphoma cells in vivo. *J Exp Med*, 200(9):1157–65, 2004.

[7] B. Brooks, D. M. Briggs, N. C. Eastmond, D. G. Fernig, and J. W. Coleman. Presentation of ifn-gamma to nitric oxide-producing cells: a novel function for mast cells. *J Immunol*, 164(2):573–9, 2000.

[8] M. Buntinx, M. Moreels, F. Vandenabeele, I. Lambrichts, J. Raus, P. Steels, P. Stinissen, and M. Ameloot. Cytokine-induced cell death in human oligodendroglial cell lines: I. synergistic effects of ifn-gamma and tnf-alpha on apoptosis. *J Neurosci Res*, 76(6):834–45, 2004.

[9] D. Burzyn, W. Kuswanto, D. Kolodin, J. L. Shadrach, M. Cerletti, Y. Jang, E. Sefik, T. G. Tan, A. J. Wagers, C. Benoist, and D. Mathis. A special population of regulatory t cells potentiates muscle repair. *Cell*, 155(6):1282–95, 2013.

[10] L. Cai, C. K. Dalal, and M. B. Elowitz. Frequency-modulated nuclear localization bursts coordinate gene regulation. *Nature*, 455(7212):485–90, 2008.

[11] F. Castellino, A. Y. Huang, G. Altan-Bonnet, S. Stoll, C. Scheinecker, and R. N. Germain. Chemokines enhance immunity by guiding naive cd8+ t cells to sites of cd4+ t cell-dendritic cell interaction. *Nature*, 440(7086):890–5, 2006.

[12] S. H. Chen, W. Forrester, and G. Lahav. Schedule-dependent interaction between anticancer treatments. *Science*, 351(6278):1204–8, 2016.

[13] F. Cofano, A. Fassio, G. Cavallo, and S. Landolfo. Binding of murine 125i-labelled natural interferon-gamma to murine cell receptors. *J Gen Virol*, 67 (Pt 6):1205–9, 1986.

[14] M. J. de Veer, M. Holko, M. Frevel, E. Walker, S. Der, J. M. Paranjape, R. H. Silverman, and B. R. G. Williams. Functional classification of interferon-stimulated genes identified using microarrays. *Journal of Leukocyte Biology*, 69(6):912–920, 2001.

[15] S. D. Der, A. Zhou, B. R. Williams, and R. H. Silverman. Identification of genes differentially regulated by interferon alpha, beta, or gamma using oligonucleotide arrays. *Proc Natl Acad Sci U S A*, 95(26):15623–8, 1998.

[16] A. S. Dighe, E. Richards, L. J. Old, and R. D. Schreiber. Enhanced in vivo growth and resistance to rejection of tumor cells expressing dominant negative ifn gamma receptors. *Immunity*, 1(6):447–56, 1994.

[17] S. Dubois, J. Mariner, T. A. Waldmann, and Y. Tagaya. Il-15ralpha recycles and presents il-15 in trans to neighboring cells. *Immunity*, 17(5):537–47, 2002.

[18] S. Dupuis, E. Jouanguy, S. Al-Hajjar, C. Fieschi, I. Z. Al-Mohsen, S. Al-Jumaah, K. Yang, A. Chapgier, C. Eidenschenk, P. Eid, A. Al Ghonaium, H. Tufenkeji, H. Frayha, S. Al-Gazlan, H. Al-Rayes, R. D. Schreiber, I. Gresser, and J. L. Casanova. Impaired response to interferon-alpha/beta and lethal viral disease in human stat1 deficiency. *Nat Genet*, 33(3):388–91, 2003.

[19] J. G. Egen, A. G. Rothfuchs, C. G. Feng, N. Winter, A. Sher, and R. N. Germain. Macrophage and t cell dynamics during the development and disintegration of mycobacterial granulomas. *Immunity*, 28(2):271–84, 2008.

[20] R. Elkon, E. Zlotorynski, K. I. Zeller, and R. Agami. Major role for mrna stability in shaping the kinetics of gene induction. *BMC Genomics*, 11:259, 2010.

[21] V. A. Fadok, D. L. Bratton, D. M. Rose, A. Pearson, R. A. Ezekewitz, and P. M. Henson. A receptor for phosphatidylserine-specific clearance of apoptotic cells. *Nature*, 405(6782):85–90, 2000.

[22] M. A. Farrar and R. D. Schreiber. The molecular cell biology of interferon-gamma and its receptor. *Annu Rev Immunol*, 11:571–611, 1993.

[23] K. Fischer, S. Voelkl, J. Berger, R. Andreesen, T. Pomorski, and A. Mackensen. Antigen recognition induces phosphatidylserine exposure on the cell surface of human cd8+ t cells. *Blood*, 108(13):4094–101, 2006.

[24] K. Gaus, E. Gratton, E. P. Kable, A. S. Jones, I. Gelissen, L. Kritharides, and W. Jessup. Visualizing lipid structure and raft domains in living cells with two-photon microscopy. *Proc Natl Acad Sci U S A*, 100(26):15554–9, 2003.

[25] Consortium Gene Ontology. Gene ontology consortium: going forward. *Nucleic Acids Res*, 43(Database issue):D1049–56, 2015.

[26] J. Gong, R. Archer, M. Brown, S. Fisher, C. Chang, M. Peacock, C. Hughes, and B. Freimark. Measuring response to therapy by near-infrared imaging of tumors using a phosphatidylserine-targeting antibody fragment. *Mol Imaging*, 12(4):244–56, 2013.

[27] S. A. Grupp, M. Kalos, D. Barrett, R. Aplenc, D. L. Porter, S. R. Rheingold, D. T. Teachey, A. Chew, B. Hauck, J. F. Wright, M. C. Milone, B. L. Levine, and C. H. June. Chimeric antigen receptor-modified t cells for acute lymphoid leukemia. *N Engl J Med*, 368(16):1509–18, 2013.

[28] Y. Hamon, C. Broccardo, O. Chambenoit, M. F. Luciani, F. Toti, S. Chaslin, J. M. Freyssinet, P. F. Devaux, J. McNeish, D. Marguet, and G. Chimini.

Abc1 promotes engulfment of apoptotic cells and transbilayer redistribution of phosphatidylserine. *Nat Cell Biol*, 2(7):399–406, 2000.

[29] D. Hanahan and R. A. Weinberg. Hallmarks of cancer: the next generation. *Cell*, 144(5):646–74, 2011.

[30] S. Hao and D. Baltimore. The stability of mrna influences the temporal order of the induction of genes encoding inflammatory molecules. *Nat Immunol*, 10(3):281–8, 2009.

[31] S. Hao and D. Baltimore. Rna splicing regulates the temporal order of tnf-induced gene expression. *Proc Natl Acad Sci U S A*, 110(29):11934–9, 2013.

[32] C. Helmstetter, M. Flossdorf, M. Peine, A. Kupz, J. Zhu, A. N. Hegazy, M. A. Duque-Correa, Q. Zhang, Y. Vainshtein, A. Radbruch, S. H. Kaufmann, W. E. Paul, T. Hofer, and M. Lohning. Individual t helper cells have a quantitative cytokine memory. *Immunity*, 42(1):108–22, 2015.

[33] A. Hoffmann, A. Levchenko, M. L. Scott, and D. Baltimore. The ikappab-nf-kappab signaling module: temporal control and selective gene activation. *Science*, 298(5596):1241–5, 2002.

[34] T. Honda, J. G. Egen, T. Lammermann, W. Kastenmuller, P. Torabi-Parizi, and R. N. Germain. Tuning of antigen sensitivity by t cell receptor-dependent negative feedback controls t cell effector function in inflamed tissues. *Immunity*, 40(2):235–47, 2014.

[35] M. P. Hosking, C. T. Flynn, and J. L. Whitton. Antigen-specific naive cd8+ t cells produce a single pulse of ifn-gamma in vivo within hours of infection, but without antiviral effect. *J Immunol*, 193(4):1873–85, 2014.

[36] O. Ilnytska, M. Santiana, N. Y. Hsu, W. L. Du, Y. H. Chen, E. G. Viktorova, G. Belov, A. Brinker, J. Storch, C. Moore, J. L. Dixon, and N. Altan-Bonnet. Enteroviruses harness the cellular endocytic machinery to remodel the host cell cholesterol landscape for effective viral replication. *Cell Host Microbe*, 14(3):281–93, 2013.

[37] E. Jouanguy, F. Altare, S. Lamhamedi, P. Revy, J. F. Emile, M. Newport, M. Levin, S. Blanche, E. Seboun, A. Fischer, and J. L. Casanova. Interferon-gamma-receptor deficiency in an infant with fatal bacille calmette-guerin infection. *N Engl J Med*, 335(26):1956–61, 1996.

[38] M. Jovanovic, M. S. Rooney, P. Mertins, D. Przybylski, N. Chevrier, R. Satija, E. H. Rodriguez, A. P. Fields, S. Schwartz, R. Raychowdhury, M. R. Mumbach, T. Eisenhaure, M. Rabani, D. Gennert, D. Lu, T. Delorey, J. S. Weissman, S. A. Carr, N. Hacohen, and A. Regev. Immunogenetics. dynamic profiling of the protein life cycle in response to pathogens. *Science*, 347(6226):1259038, 2015.

[39] Q. A. Justman, Z. Serber, Jr. Ferrell, J. E., H. El-Samad, and K. M. Shokat. Tuning the activation threshold of a kinase network by nested feedback loops. *Science*, 324(5926):509–12, 2009.

[40] W. Kastenmuller, M. Brandes, Z. Wang, J. Herz, J. G. Egen, and R. N. Germain. Peripheral prepositioning and local cxcl9 chemokine-mediated guidance orchestrate rapid memory cd8+ t cell responses in the lymph node. *Immunity*, 38(3):502–13, 2013.

[41] W. Kastenmuller, P. Torabi-Parizi, N. Subramanian, T. Lammermann, and R. N. Germain. A spatially-organized multicellular innate immune response in lymph nodes limits systemic pathogen spread. *Cell*, 150(6):1235–48, 2012.

[42] H. Kenis, H. van Genderen, A. Bennaghmouch, H. A. Rinia, P. Frederik, J. Narula, L. Hofstra, and C. P. Reutelingsperger. Cell surface-expressed phosphatidylserine and annexin a5 open a novel portal of cell entry. *J Biol Chem*, 279(50):52623–9, 2004.

[43] J. Larkin, V. Chiarion-Sileni, R. Gonzalez, J. J. Grob, C. L. Cowey, C. D. Lao, D. Schadendorf, R. Dummer, M. Smylie, P. Rutkowski, P. F. Ferrucci, A. Hill, J. Wagstaff, M. S. Carlino, J. B. Haanen, M. Maio, I. Marquez-Rodas, G. A. McArthur, P. A. Ascierto, G. V. Long, M. K. Callahan, M. A. Postow, K. Grossmann, M. Sznol, B. Dreno, L. Bastholt, A. Yang, L. M. Rollin, C. Horak, F. S. Hodi, and J. D. Wolchok. Combined nivolumab and ipilimumab or monotherapy in untreated melanoma. *N Engl J Med*, 373(1):23–34, 2015.

[44] C. J. Lee, H. R. Lin, C. L. Liao, and Y. L. Lin. Cholesterol effectively blocks entry of flavivirus. *J Virol*, 82(13):6470–80, 2008.

[45] M. J. Lee, A. S. Ye, A. K. Gardino, A. M. Heijink, P. K. Sorger, G. MacBeath, and M. B. Yaffe. Sequential application of anticancer drugs enhances cell death by rewiring apoptotic signaling networks. *Cell*, 149(4):780–94, 2012.

[46] R. E. Lee, S. R. Walker, K. Savery, D. A. Frank, and S. Gaudet. Fold change of nuclear nf-kappab determines tnf-induced transcription in single cells. *Mol Cell*, 53(6):867–79, 2014.

[47] K. Lim, Y. M. Hyun, K. Lambert-Emo, T. Capece, S. Bae, R. Miller, D. J. Topham, and M. Kim. Neutrophil trails guide influenza-specific cd8(+) t cells in the airways. *Science*, 349(6252):aaa4352, 2015.

[48] L. G. Lima, R. Chammas, R. Q. Monteiro, M. E. Moreira, and M. A.

Barcinski. Tumor-derived microvesicles modulate the establishment of metastatic melanoma in a phosphatidylserine-dependent manner. *Cancer Lett*, 283(2):168–75, 2009.

[49] B. E. Lippitz. Cytokine patterns in patients with cancer: a systematic review. *Lancet Oncol*, 14(6):e218–28, 2013.

[50] Y. Liu, L. Wang, T. Kikuiri, K. Akiyama, C. Chen, X. Xu, R. Yang, W. Chen, S. Wang, and S. Shi. Mesenchymal stem cell-based tissue regeneration is governed by recipient t lymphocytes via ifn-gamma and tnf-alpha. *Nat Med*, 17(12):1594–601, 2011.

[51] H. Lortat-Jacob and J. A. Grimaud. Interferon-gamma binds to heparan sulfate by a cluster of amino acids located in the c-terminal part of the molecule. *FEBS Lett*, 280(1):152–4, 1991.

[52] J. M. Lund, L. Hsing, T. T. Pham, and A. Y. Rudensky. Coordination of early protective immunity to viral infection by regulatory t cells. *Science*, 320(5880):1220–4, 2008.

[53] M. Miyanishi, K. Tada, M. Koike, Y. Uchiyama, T. Kitamura, and S. Nagata. Identification of tim4 as a phosphatidylserine receptor. *Nature*, 450(7168):435–9, 2007.

[54] K. J. Moore and I. Tabas. Macrophages in the pathogenesis of atherosclerosis. *Cell*, 145(3):341–55, 2011.

[55] S. Mostafavi, H. Yoshida, D. Moodley, H. LeBoite, K. Rothamel, T. Raj, C. J. Ye, N. Chevrier, S. Y. Zhang, T. Feng, M. Lee, J. L. Casanova, J. D. Clark, M. Hegen, J. B. Telliez, N. Hacohen, P. L. De Jager, A. Regev, D. Mathis,

C. Benoist, and Consortium Immunological Genome Project. Parsing the interferon transcriptional network and its disease associations. *Cell*, 164(3):564–78, 2016.

[56] P. J. Murray and T. A. Wynn. Protective and pathogenic functions of macrophage subsets. *Nat Rev Immunol*, 11(11):723–37, 2011.

[57] I. R. Nabi and P. U. Le. Caveolae/raft-dependent endocytosis. *J Cell Biol*, 161(4):673–7, 2003.

[58] D. E. Nelson, A. E. Ihekwaba, M. Elliott, J. R. Johnson, C. A. Gibney, B. E. Foreman, G. Nelson, V. See, C. A. Horton, D. G. Spiller, S. W. Edwards, H. P. McDowell, J. F. Unitt, E. Sullivan, R. Grimley, N. Benson, D. Broomhead, D. B. Kell, and M. R. White. Oscillations in nf-kappab signaling control the dynamics of gene expression. *Science*, 306(5696):704–8, 2004.

[59] D. P. Noren, W. H. Chou, S. H. Lee, A. A. Qutub, A. Warmflash, D. S. Wagner, A. S. Popel, and A. Levchenko. Endothelial cells decode vegf-mediated ca2+ signaling patterns to produce distinct functional responses. *Sci Signal*, 9(416):ra20, 2016.

[60] W. W. Overwijk, M. R. Theoret, S. E. Finkelstein, D. R. Surman, L. A. de Jong, F. A. Vyth-Dreese, T. A. Dellemijn, P. A. Antony, P. J. Spiess, D. C. Palmer, D. M. Heimann, C. A. Klebanoff, Z. Yu, L. N. Hwang, L. Feigenbaum, A. M. Kruisbeek, S. A. Rosenberg, and N. P. Restifo. Tumor regression and autoimmunity after reversal of a functionally tolerant state of self-reactive cd8+ t cells. *J Exp Med*, 198(4):569–80, 2003.

[61] A. L. Paek, J. C. Liu, A. Loewer, W. C. Forrester, and G. Lahav. Cell-to-

cell variation in p53 dynamics leads to fractional killing. *Cell*, 165(3):631–42, 2016.

[62] D. Pincus, A. Aranda-Diaz, I. A. Zuleta, P. Walter, and H. El-Samad. Delayed ras/pka signaling augments the unfolded protein response. *Proc Natl Acad Sci U S A*, 111(41):14800–5, 2014.

[63] B. Piqueras, J. Connolly, H. Freitas, A. K. Palucka, and J. Banchereau. Upon viral exposure, myeloid and plasmacytoid dendritic cells produce 3 waves of distinct chemokines to recruit immune effectors. *Blood*, 107(7):2613–8, 2006.

[64] D. L. Porter, W. T. Hwang, N. V. Frey, S. F. Lacey, P. A. Shaw, A. W. Loren, A. Bagg, K. T. Marcucci, A. Shen, V. Gonzalez, D. Ambrose, S. A. Grupp, A. Chew, Z. Zheng, M. C. Milone, B. L. Levine, J. J. Melenhorst, and C. H. June. Chimeric antigen receptor t cells persist and induce sustained remissions in relapsed refractory chronic lymphocytic leukemia. *Sci Transl Med*, 7(303):303ra139, 2015.

[65] A. Puel, S. Cypowyj, J. Bustamante, J. F. Wright, L. Liu, H. K. Lim, M. Migaud, L. Israel, M. Chrabieh, M. Audry, M. Gumbleton, A. Toulon, C. Bodemer, J. El-Baghdadi, M. Whitters, T. Paradis, J. Brooks, M. Collins, N. M. Wolfman, S. Al-Muhsen, M. Galicchio, L. Abel, C. Picard, and J. L. Casanova. Chronic mucocutaneous candidiasis in humans with inborn errors of interleukin-17 immunity. *Science*, 332(6025):65–8, 2011.

[66] J. E. Purvis, K. W. Karhohs, C. Mock, E. Batchelor, A. Loewer, and G. Lahav. p53 dynamics control cell fate. *Science*, 336(6087):1440–4, 2012.

[67] M. Rabani, J. Z. Levin, L. Fan, X. Adiconis, R. Raychowdhury, M. Garber, A. Gnirke, C. Nusbaum, N. Hacohen, N. Friedman, I. Amit, and A. Regev.

Metabolic labeling of rna uncovers principles of rna production and degradation dynamics in mammalian cells. *Nat Biotechnol*, 29(5):436–42, 2011.

[68] M. Rabani, R. Raychowdhury, M. Jovanovic, M. Rooney, D. J. Stumpo, A. Pauli, N. Hacohen, A. F. Schier, P. J. Blackshear, N. Friedman, I. Amit, and A. Regev. High-resolution sequencing and modeling identifies distinct dynamic rna regulatory strategies. *Cell*, 159(7):1698–710, 2014.

[69] S. Ran, A. Downes, and P. E. Thorpe. Increased exposure of anionic phospholipids on the surface of tumor blood vessels. *Cancer Res*, 62(21):6132–40, 2002.

[70] M. Rusnati, C. Urbinati, E. Tanghetti, P. Dell'Era, H. Lortat-Jacob, and M. Presta. Cell membrane gm1 ganglioside is a functional coreceptor for fibroblast growth factor 2. *Proc Natl Acad Sci U S A*, 99(7):4367–72, 2002.

[71] R. Sadir, E. Forest, and H. Lortat-Jacob. The heparan sulfate binding sequence of interferon-gamma increased the on rate of the interferon-gamma-interferon-gamma receptor complex formation. *J Biol Chem*, 273(18):10919–25, 1998.

[72] E. Saesen, S. Sarrazin, C. Laguri, R. Sadir, D. Maurin, A. Thomas, A. Imberty, and H. Lortat-Jacob. Insights into the mechanism by which interferon-gamma basic amino acid clusters mediate protein binding to heparan sulfate. *J Am Chem Soc*, 135(25):9384–90, 2013.

[73] K. Schroder, P. J. Hertzog, T. Ravasi, and D. A. Hume. Interferon-gamma: an overview of signals, mechanisms and functions. *J Leukoc Biol*, 75(2):163–89, 2004.

[74] E. G. Schulz, L. Mariani, A. Radbruch, and T. Hofer. Sequential polarization and imprinting of type 1 t helper lymphocytes by interferon-gamma and interleukin-12. *Immunity*, 30(5):673–83, 2009.

[75] B. Schwanhausser, D. Busse, N. Li, G. Dittmar, J. Schuchhardt, J. Wolf, W. Chen, and M. Selbach. Global quantification of mammalian gene expression control. *Nature*, 473(7347):337–42, 2011.

[76] K. Segawa, J. Suzuki, and S. Nagata. Constitutive exposure of phosphatidylserine on viable cells. *Proc Natl Acad Sci U S A*, 108(48):19246–51, 2011.

[77] A. K. Shalek, R. Satija, J. Shuga, J. J. Trombetta, D. Gennert, D. Lu, P. Chen, R. S. Gertner, J. T. Gaublomme, N. Yosef, S. Schwartz, B. Fowler, S. Weaver, J. Wang, X. Wang, R. Ding, R. Raychowdhury, N. Friedman, N. Hacohen, H. Park, A. P. May, and A. Regev. Single-cell rna-seq reveals dynamic paracrine control of cellular variation. *Nature*, 510(7505):363–9, 2014.

[78] V. Shankaran, H. Ikeda, A. T. Bruce, J. M. White, P. E. Swanson, L. J. Old, and R. D. Schreiber. Ifngamma and lymphocytes prevent primary tumour development and shape tumour immunogenicity. *Nature*, 410(6832):1107–11, 2001.

[79] Y. Shen, M. Barros, T. Vennemann, D. T. Gallagher, Y. Yin, S. B. Linden, R. D. Heselpoth, D. J. Spencer, D. M. Donovan, J. Moult, V. A. Fischetti, F. Heinrich, M. Losche, and D. C. Nelson. A bacteriophage endolysin that eliminates intracellular streptococci. *Elife*, 5, 2016.

[80] K. Simons and D. Toomre. Lipid rafts and signal transduction. *Nat Rev Mol Cell Biol*, 1(1):31–9, 2000.

[81] A. Snyder, V. Makarov, T. Merghoub, J. Yuan, J. M. Zaretsky, A. Desrichard, L. A. Walsh, M. A. Postow, P. Wong, T. S. Ho, T. J. Hollmann, C. Bruggeman, K. Kannan, Y. Li, C. Elipenahli, C. Liu, C. T. Harbison, L. Wang, A. Ribas, J. D. Wolchok, and T. A. Chan. Genetic basis for clinical response to ctla-4 blockade in melanoma. *N Engl J Med*, 371(23):2189–99, 2014.

[82] M. H. Sung, N. Li, Q. Lao, R. A. Gottschalk, G. L. Hager, and I. D. Fraser. Switching of the relative dominance between feedback mechanisms in lipopolysaccharide-induced nf-kappab signaling. *Sci Signal*, 7(308):ra6, 2014.

[83] H. Suzuki, J. A. Punt, L. G. Granger, and A. Singer. Asymmetric signaling requirements for thymocyte commitment to the cd4+ versus cd8+ t cell lineages: a new perspective on thymic commitment and selection. *Immunity*, 2(4):413–25, 1995.

[84] S. Tavazoie, J. D. Hughes, M. J. Campbell, R. J. Cho, and G. M. Church. Systematic determination of genetic network architecture. *Nat Genet*, 22(3):281–5, 1999.

[85] S. Tay, J. J. Hughey, T. K. Lee, T. Lipniacki, S. R. Quake, and M. W. Covert. Single-cell nf-kappab dynamics reveal digital activation and analogue information processing. *Nature*, 466(7303):267–71, 2010.

[86] S. M. van den Eijnde, M. J. van den Hoff, C. P. Reutelingsperger, W. L. van Heerde, M. E. Henfling, C. Vermeij-Keers, B. Schutte, M. Borgers, and F. C. Ramaekers. Transient expression of phosphatidylserine at cell-cell contact areas is required for myotube formation. *J Cell Sci*, 114(Pt 20):3631–42, 2001.

[87] G. van Meer, D. R. Voelker, and G. W. Feigenson. Membrane lipids: where they are and how they behave. *Nat Rev Mol Cell Biol*, 9(2):112–24, 2008.

[88] N. Wang, D. L. Silver, C. Thiele, and A. R. Tall. Atp-binding cassette transporter a1 (abca1) functions as a cholesterol efflux regulatory protein. *J Biol Chem*, 276(26):23742–7, 2001.

[89] S. F. Wolf, P. A. Temple, M. Kobayashi, D. Young, M. Dicig, L. Lowe, R. Dzialo, L. Fitz, C. Ferenz, R. M. Hewick, and et al. Cloning of cdna for natural killer cell stimulatory factor, a heterodimeric cytokine with multiple biologic effects on t and natural killer cells. *J Immunol*, 146(9):3074–81, 1991.

[90] M. R. Zaidi and G. Merlino. The two faces of interferon-gamma in cancer. *Clin Cancer Res*, 17(19):6118–24, 2011.

[91] J. Zhu, H. Yamane, and W. E. Paul. Differentiation of effector cd4 t cell populations (*). *Annu Rev Immunol*, 28:445–89, 2010.